



Magnetotelluric 3-D inversion—a review of two successful workshops on forward and inversion code testing and comparison

Marion P. Miensopust,^{1,2,*} Pilar Queralt,³ Alan G. Jones¹ and the 3D MT modellers[†]

¹Dublin Institute for Advanced Studies, School of Cosmic Physics, Dublin, Ireland. E-mail: Marion.Miensopust@bgr.de

²Institut für Geophysik, Westfälische Wilhelms-Universität Münster, Germany

³Departament Geodinàmica i Geofísica, Universitat de Barcelona, Spain

Accepted 2013 February 14. Received 2013 February 14; in original form 2012 May 27

SUMMARY

Over the last half decade the need for, and importance of, three-dimensional (3-D) modelling of magnetotelluric (MT) data have increased dramatically and various 3-D forward and inversion codes are in use and some have become commonly available. Comparison of forward responses and inversion results is an important step for code testing and validation prior to ‘production’ use. The various codes use different mathematical approximations to the problem (finite differences, finite elements or integral equations), various orientations of the coordinate system, different sign conventions for the time dependence and various inversion strategies. Additionally, the obtained results are dependent on data analysis, selection and correction as well as on the chosen mesh, inversion parameters and regularization adopted, and therefore, a careful and knowledge-based use of the codes is essential. In 2008 and 2011, during two workshops at the Dublin Institute for Advanced Studies over 40 people from academia (scientists and students) and industry from around the world met to discuss 3-D MT inversion. These workshops brought together a mix of code writers as well as code users to assess the current status of 3-D modelling, to compare the results of different codes, and to discuss and think about future improvements and new aims in 3-D modelling. To test the numerical forward solutions, two 3-D models were designed to compare the responses obtained by different codes and/or users. Furthermore, inversion results of these two data sets and two additional data sets obtained from unknown models (secret models) were also compared. In this manuscript the test models and data sets are described (supplementary files are available) and comparisons of the results are shown. Details regarding the used data, forward and inversion parameters as well as computational power are summarized for each case, and the main discussion points of the workshops are reviewed. In general, the responses obtained from the various forward models are comfortably very similar, and discrepancies are mainly related to the adopted mesh. For the inversions, the results show how the inversion outcome is affected by distortion and the choice of errors, as well as by the completeness of the data set. We hope that these compilations will become useful not only for those that were involved in the workshops, but for the entire MT community and also the broader geoscience community who may be interested in the resolution offered by MT.

Key words: Numerical solutions; Inverse theory; Magnetotelluric; Geomagnetic induction.

1 INTRODUCTION

Testing and validation of new approaches and techniques are essential, and therefore, measures to verify electromagnetic (EM) forward and inversion algorithms are required. Within the geoscientific EM community, several prior workshops and projects dealt with comparison of results obtained from test models or of data sets designed by teams or individuals to address specific tasks (i.e. 2-D forward modelling, 3-D forward modelling). These results were calculated by different users applying different algorithms and

* Now at: Federal Institute for Geosciences and Natural Resources, Hannover, Germany.

† Dmitry Avdeev, Anna Avdeeva, Ralph-Uwe Börner, David Bosch, Gary Egbert, Colin Farquharson, Antje Franke-Börner, Xavier Garcia, Nuree Han, Sophie Hautot, Elliot Holtham, Juliane Hübner, David Khoza, Duygu Kiyan, Florian Le Pape, Juanjo Lledo, Tae Jong Lee, Randall Mackie, Anna Martí, Naser Meqbel, Greg Newman, Doug Oldenburg, Oriol Rosell, Yutaka Sasaki, Weerachai Siripunvaraporn, Pascal Tarits and Jan Vozar.

approaches to allow for comparison amongst each other. The success of such workshops and projects lies not only in the value of the models and data sets but also in the active participation of scientists attending and contributing to these comparisons. One of the first and the most important ones was COMMEMI (Comparison Of Modelling Methods for ElectroMagnetic Induction) that was proposed and adopted at the VI EMI International Workshop (Victoria, B.C., Canada, 1982) (Zhdanov *et al.* 1997). The project comprises a set of six 2-D and two 3-D models covering a wide range of resistivity contrasts and structures. It includes a simple model, for which an analytical solution exists, as well as a highly complex model that represents a structure very similar to a real geological setting. The main contribution of this project was to assemble the numerical forward solutions for these models, and some of them have since become the standard models for testing new approaches and algorithms.

During the 1990s, five Magnetotelluric Data Interpretation Workshops took place namely MT-DIW1 in Wellington, New Zealand, 1992; MT-DIW2 in Cambridge, England, 1994; MT-DIW3 in Tsukuba, Japan, 1996; MT-DIW4 in Sinaia, Romania, 1998 and MT-DIW5 in Cabo Frio, Brazil, 2000. Together with a comparison of the inversion models, the main contributions of these workshops were the data sets provided for the interpretation exercise. For the first workshops, MT-DIW1 and MT-DIW2, two profiles of real data—COPROD2 and BC87 (Jones 1993a,b)—were examined. There are a large number of publications using these data to test 2-D inversion codes and different techniques for MT data decomposition. The results of those workshops are published as special sections in the *Journal of Geomagnetism and Geoelectricity*, volume 45(9) (1993) and 49(6) (1997) with summaries by Jones (1993c) and Jones & Schultz (1997) and a comparison of all 2-D models presented at the MT-DIW1 workshop by Jones (1993a). For the subsequent workshops (MT-DIW3, MT-DIW4 and MT-DIW5) the Kayabe data set was provided consisting of 209 stations on a rectangular grid. This data set allowed testing different approaches of handling 3-D MT data as well as studying the errors introduced by 2-D interpretation of 3-D bodies (i.e. Garcia *et al.* 1999). Also, two synthetic data sets (COPROD2S1 and COPROD2S2) were created for MT-DIW4 and MT-DIW5. COPROD2S1 is error-free, whereas COPROD2S2 contains added noise and static shifts. They are very valuable to compare inversion procedures (Varentsov 1998). All these data sets with full information can be downloaded from: <http://mtnet.dias.ie/workshops/mt-diw> (last accessed 1 March 2013).

In parallel, the 3-D EM International Symposium was established, not to compare models and results, but to stimulate symbiosis and gather information about new developments to improve approaches and techniques used in 3-D: 3DEM-1 (Ridgefield, USA, 1995); 3DEM-2 (Salt Lake City, USA, 1999); 3DEM-3 (Adelaide, Australia, 2003); 3DEM-4 (Freiberg, Germany, 2007) and 3DEM-5 (soon in Sapporo, Japan, May 2013). These symposia covering 3-D EM modelling, inversion and application are a record of the growing interest in 3-D EM modelling and inversion methods.

The EM Induction workshop reviews are also worth highlighting as they offer a thorough summary of the state of the art for specific subjects in a format addressed to the entire community, not only specialists. In 1988, at the EM Induction workshop in Sochi (Russia), Červ & Pek (1990) presented a review on some aspects of modelling EM fields in 3-D inhomogeneous media considering various 3-D modelling techniques and their comparison. At the same workshop, Oldenburg (1990) focused on new techniques of EM data inversion especially related to the 2-D MT problem. In

2002, at the workshop in Santa Fe (USA), Ledo (2006) gave an excellent review about 3-D effects on 2-D interpretations. At the following EM Induction workshop (2004) in Hyderabad (India), Avdeev (2005) presented a review concentrating on recent developments in the finite-difference (FD), finite element (FE) and integral equation (IE) methods for 3-D forward modelling and inversion. He also included an overview of certain optimization procedures. At the 2008 workshop in Beijing (China), Börner (2010) gave a review of numerical solutions of 3-D EM forward modelling, and he addressed several challenges in reducing the computing costs in terms of code efficiency and speed. In Giza (Egypt) at the 2010 workshop, Siripunvaraporn (2012) reviewed 3-D magnetotelluric data inversion techniques, summarizing work done related to various optimization methods and provides a comparison of those. Finally, at the most recent workshop (2012) held in Darwin (Australia), two more modelling reviews followed: one on joint inversion by Haber and the other one on parallel computing by Newman.

There is significantly increased interest and awareness in 3-D modelling and inversion, and the efforts to develop 3-D codes have increased and the number of projects and publications presenting 3-D MT data is rising quickly (i.e. Chave & Jones 2012, and references therein). Nevertheless, 3-D approaches and algorithms are not yet standard tools for MT data modelling and inversion, and numerous issues remain to be addressed to avoid pitfalls by ill-informed users. These start with simple things, like a comparison of the forward responses calculated by different codes and by different users, to more applied issues, like the question of which strategies to use for the inversion of a large data set, but also more complex problems as, for example, how to handle distortion in 3-D environments (e.g. Jones 2011). Combining the idea of COMMEMI and the MT Data Interpretation Workshops, the first 3-D MT Inversion Workshop was held on 2008 March 12–14 in Dublin, Ireland. It was such a success that the 3-D MT Inversion Workshop II followed on 2011 March 30 to April 1 (again in Dublin).

The workshops are designed to be an opportunity to bring together a mix of MT 3-D inversion code writers and users and see how well the codes perform as well as how good the understanding of how to use them is. The main topics of the workshops were to assess the state of the art, to compare the results of the codes, and think about future improvements and new aims in 3-D modelling and inversion. Prior to each workshop, first, a test model and secondly a test data set retrieved from a secret model were distributed, so that forward modelling and inversion could be performed in advance and the results were available for comparison during the workshop. During both workshops, a total of 42 people from industry and academia participated, most attending both workshops, and made the workshops such a success. Herein the main results of both 3-D MT Inversion Workshops will be presented showing some representative sites and model slices (see supplementary files for more information available). The discussion summarizes issues related to the presented test data sets and models as well as reflects some of the points that were raised at the open discussions during both workshop.

2 FORWARD MODELLING

The first task for the attendees of the two workshops was to forward model a given 3-D electrical conductivity structure and obtain synthetic data at given locations and periods. In the following we will briefly describe the different techniques and codes used. Then, the models and instructions are represented and finally the results are illustrated and compared.

2.1 Different algorithms and approaches

The participants of the workshops used different numerical algorithms, based on FD, FE or IE methods, to calculate the 3-D forward responses. To solve the problem, all of these codes use numerical approximations of the Maxwell's equations in the frequency domain. The most commonly employed method for our comparison was FD; namely the codes by Mackie *et al.* (1994), Newman & Alumbaugh (2000), Sasaki (2001), Farquharson *et al.* (2002), Siripunvaraporn *et al.* (2002), Egbert & Kelbert (2012) and Börner (personal communication). Using the FD approach, the electrical properties of the Earth and the EM fields or their potentials are sampled over a rectangular mesh and the associated differential equations are approximated by FDs resulting in a system of linear equations to solve. However, there are important differences between the various codes; for example, the solvers applied to the system of linear equations, the type of grid and boundary conditions used. It is beyond the scope of this paper to compare the technical aspects of the different codes (the interested reader may consult the above references for more details). Despite these differences, the design of an appropriate mesh is absolutely crucial and affects the derived results significantly.

Although the number of available MT forward codes based on FE and IE approaches is limited, some attendees obtained responses using such codes (i.e. FE: Franke *et al.* (2007), Nam *et al.* (2007), Farquharson & Miensopust (2011); IE: Avdeev *et al.* (2002)). The numerical implementations of FE and IE are more complex than FD, and often require a highly detailed knowledge of the algorithm to use it successfully. These two methods represent extreme situations: IE is efficient for models with a localized anomalous conductivity in a 1-D background given that only the anomalous region needs to be discretized. In contrast, FE methods are powerful for modelling complex media with the inclusion of detailed topography. The code of Avdeev *et al.* (2002) is based on the IE approach to describe Maxwell's differential equations and applies the Green's function technique to obtain the scattering equation. In this way, only the volume where the conductivity is different from the background requires discretization and results in a linear equation system of reduced size. The FE method is based on the approximation of the EM fields, or their potentials, by a set of nodal- or edge-element basis functions. Either Galerkin's method or the FE analysis of the weak form of the MT boundary value problem yields a discrete approximation and results in a system of linear equations. As in the FD case, there are similar differences between the FE codes used for the comparison (e.g. the applied solver, the type of grid and boundary conditions used). Additionally, the discretization can be implemented in different ways, for example, as rectilinear mesh, structured mesh of hexahedral elements (i.e. distorted bricks) and unstructured grids of tetrahedral elements. Furthermore, the type of basis function used (i.e. nodal or edge), as well as its order, varies depending on the code. (For more details, the interested reader is referred to the above references of the various codes.)

Note that all of the codes used do not mimic field acquisition correctly, in that electric field calculations in the codes are made for a point in space, whereas in the field the electric fields are derived by measuring the potential differences between two points in the ground, typically 100 m apart. See Jones (1988) and Poll *et al.* (1989) for a discussion of this issue.

2.2 Dublin Test Model 1 (DTM1)

The design of the forward model for the first workshop was aimed at a comparison of forward responses obtained from various codes and

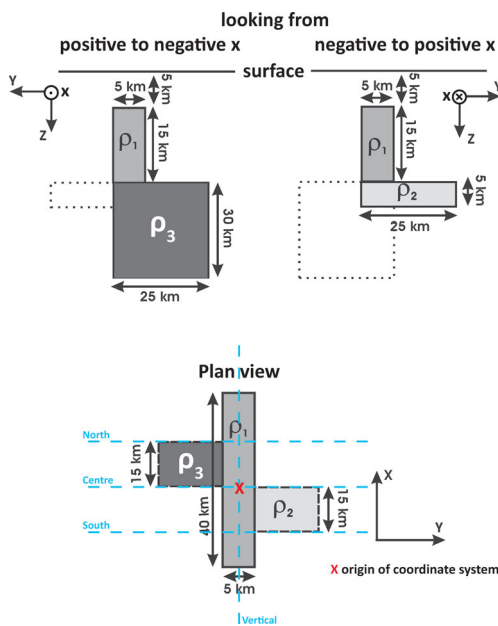


Figure 1. Sketch of Dublin Test Model 1 (DTM1). On top two sections are shown, one across body 3 (left) and one across body 2 (right). Additionally, a plan view of all three bodies is shown. The background is a $100 \Omega\text{m}$ homogeneous half-space and the dimensions and resistivities of the blocks are listed in Table 1. The blue dashed lines represent the four profiles with 5-km site spacing (North, Centre, South: 16 sites each, Vertical: 11 sites).

Table 1. Dimensions and resistivity values of the three blocks in the Dublin Test Model 1 (DTM1). For x -, y - and z -direction, the extent of the blocks is specified.

	x (km)	y (km)	z (km)	resistivity (Ωm)
body 1	-20 to 20	-2.5 to 2.5	5 to 20	10
body 2	-15 to 0	-2.5 to 22.5	20 to 25	1
body 3	0 to 15	-22.5 to 2.5	20 to 50	10 000

different users, but also to see how they dealt with strong resistivity contrasts. The 3-D forward model consists of three different blocks embedded in a homogeneous, $100 \Omega\text{m}$ half-space. Fig. 1 shows diagrams of the structure in section and plan view. Table 1 summarizes the dimensions and resistivity values of the three bodies. The origin of the coordinate system is defined at the centre (in lateral direction) of body 1, and is a right-handed system with z positive downwards. The sites are located on four profiles (see Fig. 1). Three are parallel to the y -direction at $x = -15, 0, 15$ km with 16 equally distributed sites with 5 km spacing from -37.5 to 37.5 km. The fourth profile is parallel to the x -direction at $y = 0$ km and has 11 sites from -25 to 25 km (also 5-km site spacing). The task was to calculate the forward responses at all sites for the period range of 0.1 s to 10 000 s at four periods per decade.

Table 2 lists, for all forward response sets, the name of the user(s), the code and information about the mesh and calculation times whereas the obtained response curves of an example site ($x = y = 0$ km), which is considered as representative for the discrepancies between different results, are shown in Fig. 2. From top to bottom, each row of this figure shows the xx , xy , yx and yy components (i.e. resistivity and phase curves). Each column highlights a group of responses in colour, whereas the respective other responses are shown in grey. The first column presents results from different people using the FD code of Farquharson *et al.* (2002) (contoured colour symbols) and the FD code of Mackie *et al.*

Table 2. List of DTM1 forward results. The code and its type (finite-difference FD or finite-element FE) as well as the user are specified. Further more the used mesh (i.e. number of cells in each direction and—if available—in parentheses the lateral width of the centre cells), required CPU time (and target tolerance TT or achieved tolerance AT) and the specification of the used computer are listed.

Code	User	Mesh (# of cells)	CPU time and tolerance AT/TT	Computer used
FD (Egbert & Kelbert 2012)	Naser Meqbel	$42 \times 42 \times 56$ (plus 10 air layers)	—	—
FD (Farquharson <i>et al.</i> 2002) (serial)	Colin Farquharson	$72 \times 72 \times 72$ (2.5 km)	AT: 10^{-8} to 10^{-10} (low tolerance for long periods)	Mac PowerPC G5, 2 GHz
(frequency parallelization)	Elliot Holtham & Doug Oldenburg	>1 s: $44 \times 52 \times 43$ (2.5 km) ≤ 1 s: $104 \times 114 \times 46$ (0.5 km)	49 h 37 min TT: 10^{-9} (not achieved at all periods)	Dual AMD 244 Opteron CPU, 4GB RAM
(serial)	Marion Miensopust	$92 \times 58 \times 37$ (0.5–1 km)	—	—
FD (Mackie <i>et al.</i> 1994) (parallelization with PETSc: distributes linear system/not exactly domain decomposition)	Randall Mackie	$95 \times 95 \times 73$ (without air layers)	30 min TT: $10^{-10} = rtol$ $(r < rtol \cdot b)$ with $r = b - Ax$; b = right hand side; all preconditioned)	36 dual processor Xeons, 3.2 GHz
(serial)	Marion Miensopust	$85 \times 62 \times 34$ (plus 10 air layers)	51 min TT: 10^{-8}	Intel Core2 CPU E6300, 1.86 GHz, 3.25GB RAM
FD (Newman & Alumbaugh 2000) (frequency parallelization & domain decomposition; see reference)	Greg Newman	$285 \times 207 \times 125$ (0.3 km) to $161 \times 171 \times 145$ (1 km)	4 min – 38 min per period (full impedance estimation) TT: 10^{-12}	Parallel Linux cluster using 64 cores
FD (Sasaki 2001)	Yutaka Sasaki	$65 \times 83 \times 51$	1 h 14 min	Pentium 4 PC, 2GB RAM
FD (Siripunvaraporn <i>et al.</i> 2002) (serial)	Marion Miensopust	$39 \times 40 \times 18$ (1.25 km) (plus 7 air layers)	1 h 18 min TT: 10^{-7}	Intel Core2 CPU E6300, 1.86 GHz, 3.25GB RAM
FE (Nam <i>et al.</i> 2007)	Nuree Han & Tae Jong Lee	$48 \times 47 \times 31$	57 h 16 min	cluster: 256 nodes IBM x335, each 2 CPUs (Pentium IV Xeon DP 2.8 GHz)
IE (Avdeev <i>et al.</i> 2002) (serial)	Dmitry Avdeev	$120 \times 135 \times 23$	4 h 11 min	Laptop: T7200 2 GHz CPU, 2 GB RAM

(1994) (filled colour symbols). The other four FD response sets obtained from different codes (see Table 2) are shown in the middle column. The FE and IE response-curves can be found in the right column.

In general, all obtained response curves are in a good agreement with each other. Although the methods are different, and although the meshes differ substantially, the responses that Han & Lee obtained using the FE code by Nam *et al.* (2007) are almost identical with the IE responses Avdeev obtained with his code (Avdeev *et al.* 2002). Both results using the code by Mackie *et al.* (1994) agree reasonably well, and we surmise that the small discrepancies are due to the limited number of cells available in the WinGLink serial version (used by Miensopust) compared to the parallel version (used by Mackie). Sasaki's responses using his code (Sasaki 2001), the responses obtained by Meqbel using the code by Egbert & Kelbert (2012) and Newman's data obtained from the finest mesh of all using his code (Newman & Alumbaugh 2000), are also in a good agreement with the FE and IE responses. The three responses calculated using the code of Farquharson *et al.* (2002) show some obvious differences. The data set calculated by Farquharson suffers from the rather coarse mesh (2.5-km centre cells) and, therefore, has problems to estimate the responses at the short periods correctly (some data points are even outside the axes limits). Alternatively, the responses from Miensopust differ slightly for the longer periods, which is probably related to a mesh that suits the shorter periods better than the longer ones. The best data set using this code was obtained by Holtham & Oldenburg. They used two separate meshes, one very fine mesh for short periods equal or less than 1 s and a larger scale one to suit the long periods greater than 1 s. Merging the data from both meshes, they obtained good responses over the

whole period range. Due to memory limitations, the mesh used by Miensopust applying the code by Siripunvaraporn *et al.* (2002) is by far the smallest. Therefore, the discrepancy is slightly larger than for the other results. Although the differences might seem relatively large, we would like to emphasize that is not the case. It is an illusion caused by the extremely stretched axes for the xy and yx resistivities. On a normal scale, hardly any differences are visible amongst the different results; the resistivity axes were enlarged to about one decade (in contrast to five decades for the periods). Furthermore, the logarithmic scale additionally emphasises differences for small resistivity values. For example, the maximum xy resistivity value obtained for the longest period is $54.7 \Omega\text{m}$, whereas the smallest is $45.4 \Omega\text{m}$. On a normal logarithmic scale these differences would hardly be recognizable, although they would be well outside normal MT field data precision of typically 1 per cent in impedance, which is 2 per cent in apparent resistivity (approx. $\pm 1 \Omega\text{m}$).

It is also obvious that the diagonal elements have relatively large and well-defined resistivity values for long periods that are about 2 orders of magnitude smaller than those for the off-diagonals. Above 1 s, the diagonal values all match very well, but for shorter periods, when the resistivity values are below 10^{-4} to $10^{-5} \Omega\text{m}$, the phase values become more random (as expected). Therefore, for this particular case we would suggest a threshold value of $10^{-5} \Omega\text{m}$ to distinguish if the diagonal element values contain structural information, and hence should be included in an inversion, or not. For this synthetic case study, the threshold only needs to consider numerical errors, and, therefore, it is orders of magnitude below errors introduced by noise. In reality, a threshold value of $0.1 \Omega\text{m}$ is more likely to be appropriate, given typical signal-to-noise considerations.

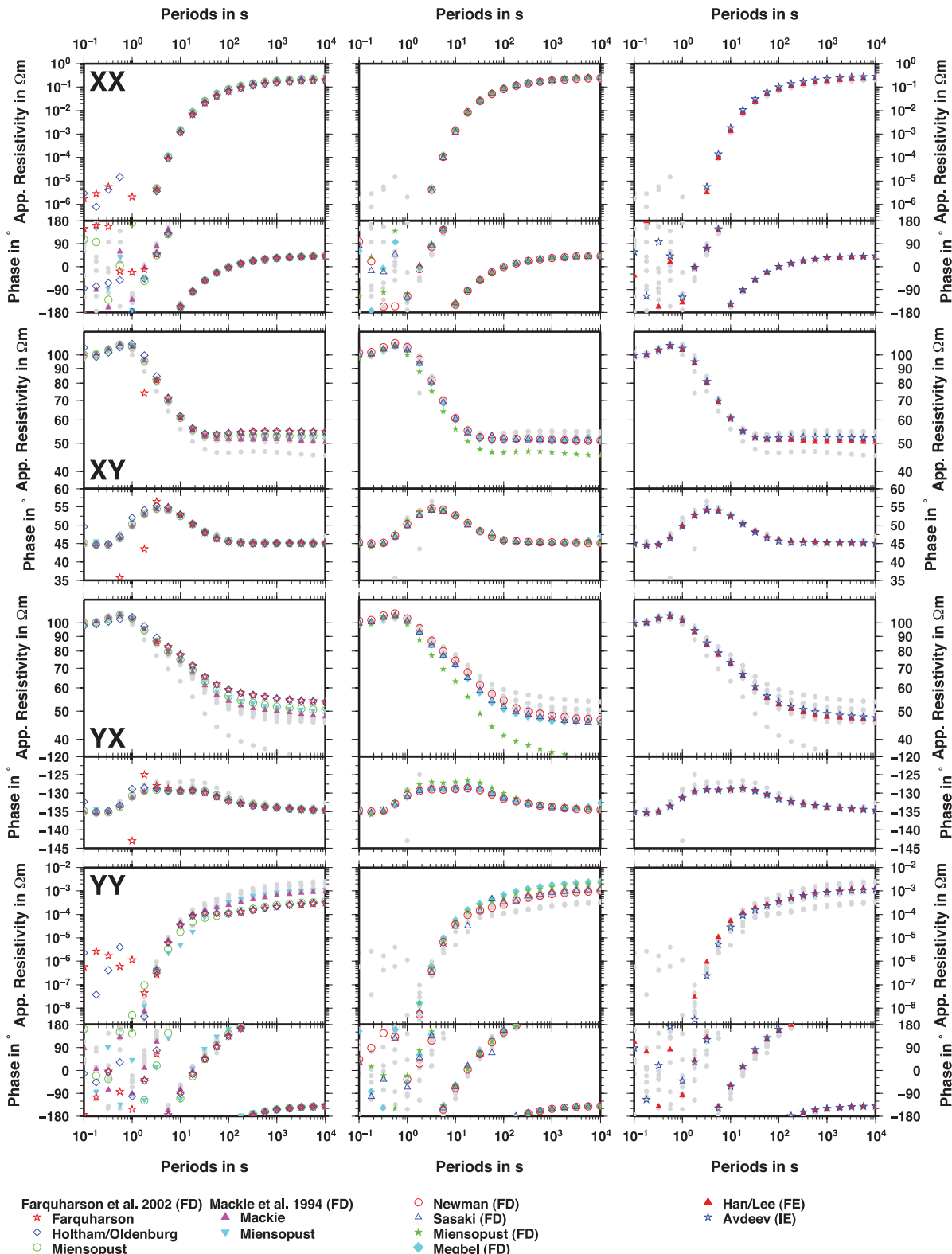


Figure 2. Comparison of the obtained DTM1 responses at an example site (central site at $x = y = 0$ km). From top to bottom each row shows the xx , xy , yx and yy components (i.e. apparent resistivity and phase curves). The left column shows in colour a comparison of responses from different users obtained using the FD codes by Farquharson *et al.* (2002) and Mackie *et al.* (1994). In the middle responses obtained by various other FD codes: Newman used the code by Newman & Alumbaugh (2000), Sasaki the one by Sasaki (2001), Miensopust the one by Siripunvaraporn *et al.* (2002) and Meqbel applied the code by Egbert & Kelbert (2012). The right column shows the responses obtained with the FE code (Nam *et al.* 2007) by Han/Lee and the IE responses of Avdeev using the code by Avdeev *et al.* (2002). In each column, the grey symbols show the respective other responses for comparison. More details can be found in Table 2 and in the text. Note that the extremely stretched xy and yx resistivity and phase axes cause exaggeration and therefore overemphasise discrepancies which would hardly be visible on a normal scale.

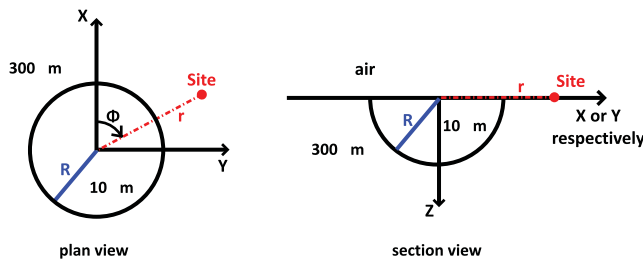


Figure 3. Sketch of Dublin Test Model 2 (DTM2). A plan view (left) and a section (right) show the structure of DTM2. The radius R is 5 km and the locations of the sites are given in Cartesian coordinates (see Table 3).

2.3 Dublin Test Model 2 (DTM2)

The motivation for the design of the forward model for the second workshop was again to compare the solutions of various codes amongst each other, but additionally to investigate how well galvanic effects are dealt with by the codes. Therefore, the 3-D forward model consists of a $10 \Omega\text{m}$ hemisphere of radius $R = 5 \text{ km}$ directly beneath the surface of a homogeneous, $300 \Omega\text{m}$ half-space (after Groom & Bailey 1991). The advantage of this structure is that there are analytical solutions at the galvanic limit (see Groom & Bailey 1991). The centre of the hemisphere is defined as the origin of the coordinate system, and Fig. 3 shows sketches of the section and plan view. One site is located at the centre of the hemisphere, all other sites are located on circles of different radii from the centre inside and outside the hemisphere. The site locations are defined in Cartesian coordinates and listed in Table 3. The task was to calculate the forward responses at all sites for a period range of 0.01–10 000 s (four periods per decade).

Table 4 lists, for all forward response sets, the name of the user(s), the code and information about the mesh and calculation times.

Table 3. Coordinates of the site locations for Dublin Test Model 2 (DTM2).

Site no.	x (m)	y (m)	Site no.	x (m)	y (m)
0	0	0	25	5500	0
1	2500	0	26	3889	3889
2	1768	1768	27	0	5500
3	0	2500	28	-3889	3889
4	-1768	1768	29	-5500	0
5	-2500	0	30	-3889	-3889
6	-1768	-1768	31	0	-5500
7	0	-2500	32	3889	-3889
8	1768	-1768	33	15 000	0
9	4500	0	34	10 607	10 607
10	3182	3182	35	0	15 000
11	0	4500	36	-10 607	10 607
12	-3182	3182	37	-15 000	0
13	-4500	0	38	-10 607	-10 607
14	-3182	-3182	39	0	-15 000
15	0	-4500	40	10 607	-10 607
16	3182	-3182	41	25 000	0
17	5100	0	42	17 678	17 678
18	3606	3606	43	0	25 000
19	0	5100	44	-17 678	17 678
20	-3606	3606	45	-25 000	0
21	-5100	0	46	-17 678	-17 678
22	-3606	-3606	47	0	-25 000
23	0	-5100	48	17 607	-17 607
24	3606	-3606			

Fig. 4 shows the obtained response curves for sites 10 and 18 (considered to be representative) in comparison to analytical solutions. First, the analytic solutions consider only the galvanic effects on the electric field (i.e. only the galvanic distortion tensor C is applied to the true impedance tensor $Z_{\text{true}} \rightarrow Z = CZ_{\text{true}}$, after Groom & Bailey 1991) and are indicated by a grey dashed line, and secondly, the full analytic solution of the galvanic scatterer was calculated by David Bosch (after Groom & Bailey 1991) and is represented by the solid black line. Note that the xx and yy components of CZ_{true} and the full analytical solution are indeterminate for sites located inside the hemisphere (e.g. site 10), and are therefore not plotted.

From top to bottom, each row of this figure shows the xx , xy and yy components (i.e. resistivity and phase curves)—on the left for site 10 and on the right for site 18. Blue symbols represent the various FD response curves, green symbols are the FE results and the IE responses are in red (more details about the different responses regarding the user, code, mesh etc. can be found in Table 4). With respect to the hemisphere's extent at the surface, site 10 is located inside the hemisphere and 500 m away from the edge of it, whereas site 18 is only 100 m away from the edge but outside the hemisphere (assuming point electric field measurements).

A structure like this one is a challenge for mesh and model design, and of particular difficulty especially for FD codes or other codes using rectilinear meshes. The blocky discretization of the hemisphere subsurface causes a large variation in the response curves at sites in its proximity (such as sites 10 and 18). For sites further away from the hemisphere, the agreement between the various responses is good, and also for sites inside the hemisphere, but with greater distance to the edge the agreement is better but still influenced by the variation in volume and the position of the bottom boundary (both cases are not shown here). Due to the proximity of sites 10 and 18 to the edge of the hemisphere, and the tangent of the edge being not parallel to the coordinate system, the diagonal elements are significant for almost all periods.

For site 18 (i.e. outside the hemisphere) all four phases are in a very good agreement for all computations (including the analytic long period limits). Inside the hemisphere (i.e. site 10) the off-diagonal phases agree well, but the diagonal phases show two groups of responses for long periods. As responses calculated by different people but the same code are present in both groups, we can exclude the possibility that the grouping is algorithm related. It rather seems to be a consequence of mesh design and the approximation of the surface of the hemisphere.

The resistivity values of all components for both sites show discrepancies (site 10 for longer periods but site 18 for all periods). Considering the distance of site 18 to the edge of the hemisphere (100 m) and the $300 \Omega\text{m}$ of the hemisphere, the edge of the hemisphere should be visible for periods longer than approximately 0.0001 s and therefore for the whole periods range as observed. Site 10 is 500 m away and, considering the $10 \Omega\text{m}$ of the hemisphere, periods longer than approximately 1 s should be affected. The reason why the responses differ for the various results is the discrepancy in the discretization of the hemisphere using different meshes. As slightly different meshes and approximations cause a different distortion, each response is basically statically shifted differently for site 18 (i.e. outside the hemisphere). This shift is strongest for the responses obtained using the coarsest, rectilinear meshes (500-m cell width compared to 250 m and less), that is, the response from Börner, Farquharson and Hübner. (In rectilinear meshes, a step-like realization of topography can introduce a similar static shift that decreases with decreasing cell size.) In general, it seems that the

Table 4. List of DTM2 forward results. The code and its type (finite-difference FD or finite-element FE) as well as the user are specified. Further more the used mesh (i.e. number of cells in each direction and—if available—in parentheses the lateral width of the centre cells), required CPU time (and target tolerance TT or achieved tolerance AT) and the specification of the used computer are listed.

Code	User	Mesh (# of cells)	CPU time & tolerance AT/TT	Computer used
FD (Börner, pers. comm.) (parallel/direct solver PARDISO)	Ralph-Uwe Börner	129 600 (500 m)	45 min	AMD Opteron6136 (2 CPUs each 4 cores, 2.4 GHz, 64 GB)
FD (Egbert & Kelbert 2012)	Naser Meqbel	96 × 96 × 45 (125 m)	35 min	parallel/51 processors
FD (Mackie <i>et al.</i> 1994) (serial)	Duygu Kiyan & David Khoza	68 × 69 × 40 (~250 m) (+ 1-D base model)	2 h 15 min TT: 10^{-8}	Dell 2 CPUs E5420@2.5 GHz, 3.25 GB
(serial)	Florian Le Pape	66 × 64 × 42 (~250 m) (+ 1-D base model)	2 h TT: 10^{-8}	Dell 2 CPUs E5420@2.5 GHz, 3.25 GB
(parallelization with PETSc: distributes linear system/not exactly domain decomposition)	Randall Mackie	85 × 85 × 59	2 h TT: $10^{-10} = rtol$ ($ r < rtol \cdot b $ with $r = b - Ax$; b = right hand side; all preconditioned)	Dell 690 workstation, Intel Xeon quad-core 5150@2.66 GHz, 4 GB
(serial)	Marion Miensopust	72 × 72 × 30 (250 m) (+ 1-D base model)	2 h TT: 10^{-8}	Dell 2 CPUs 6300@1.86 GHz, 4GB
FD (Siripunvaraporn <i>et al.</i> 2002) (serial)	Juliane Hübert	45 × 45 × 23 (500 m)	15 h	desktop: 2.6GHz, 3.5GB
FD (Siripunvaraporn & Egbert 2009) (frequency parallelization)	Jan Vozar	153 × 153 × 45	12 h TT: 10^{-7}	24 CPUs on ICHEC cluster Stokes
FE (Farquharson & Miensopust 2011) (serial)	Colin Farquharson	70 × 70 × 43 (500 m)	2 h per period (full impedance estimation) AT: from 0.01 (short periods) to 10^{-15} (long periods)	2 to 3 GB
FE (Franke <i>et al.</i> 2007) (parallel/direct solver PARDISO)	Antje Franke-Börner	~300 000 elements	6 h	AMD Opteron6136 (2 CPUs each 4 cores, 2.4 GHz, 64 GB)
IE (Avdeev <i>et al.</i> 2002) (serial)	Dmitry Avdeev	249 × 249 × 32 (~40 m) (mesh finer than needed)	56 h TT: $0.0003 > b - Ax / b $ (system of linear equations: $Ax = b$)	Intel Core i7-2630@2GHz,4GB (laptop)
(serial)	Anna Avdeeva	120 × 120 × 28 (83.3 m)	10 h TT: $0.001 \geq b - Ax / b $ (system of linear equations: $Ax = b$)	Adakus cluster (Intel Xeon X5570@2.93 GHz, 24 GB)

shift for sites inside the hemisphere (on the conductive side; e.g. site 10) tends to overestimation of the resistivity values, whereas outside (on the resistive side; e.g. site 18) resistivities are, by trend, underestimated.

3 INVERSION

The inversion tasks were of two different types; first all participants were asked to invert the data obtained from the forward model, that is, a known structure, and secondly, to deal with a data set of an unknown structure, as it would be the case for real field data. In the following we will briefly describe the different inversion algorithms that were used, and then present a comparison of the inversion results for each of the models.

3.1 Different algorithms and approaches

As the forward solver is the driving engine of an inversion algorithm, the inversion codes are also based on FD, FE and IE methods. For the inversion task of both workshops only FD (Mackie *et al.* 2001; Siripunvaraporn *et al.* 2005; Hautot *et al.* 2007, 2011; Siripunvaraporn & Egbert 2009; Egbert & Kelbert 2012) and IE (Avdeev & Avdeeva 2009; Avdeeva *et al.* 2012) codes were used. The 3-D magnetotelluric inverse problem is far from being solved, but these codes using different inversion schemes showed that one can recover the conductivity structure of simple, synthetic test models

reasonably well, to greater or less degrees depending on resolution and sensitivity. The major issues of making MT 3-D inversion a routinely applied procedure are (i) the long computation time and (ii) the requirement of fast workstations with large memories, preferably even huge clusters for parallel computation. The time-wise most expensive part is the construction of the sensitivity matrix. To avoid this time consuming procedure, different schemes were developed that use approximations of the sensitivity matrix (e.g. approximate sensitivities from a homogeneous or 1-D/layered half-space, quasi-linear approximation of Green's functions). As such approximate methods have their limitations (e.g. work best for small resistivity contrasts, and the accuracy of the inversion is questionable), they are of value but cannot replace methods based on the full solution of the EM induction equations. Methods such as the conjugate gradient (CG) or non-linear CG (NLCG) (e.g. Mackie *et al.* 2001; Hautot *et al.* 2007, 2011; Egbert & Kelbert 2012) and Quasi-Newton (QN) methods (e.g. Avdeev & Avdeeva 2009; Avdeeva *et al.* 2012) avoid both the explicit computation and storage of a full sensitivity matrix. Only the gradient vector of the objective functional is needed. Other codes are based on a Gauss-Newton-type (GN) approach in model or data space (e.g. Siripunvaraporn *et al.* 2005; Siripunvaraporn & Egbert 2009). Some of these codes are written using OPENMP or the message passing interface (MPI) protocol or similar to make them run on PC-clusters or massively parallel systems in order to reduce the computation time. In the review paper by Siripunvaraporn (2012), the different approaches are described in more detail (also see the individual references of

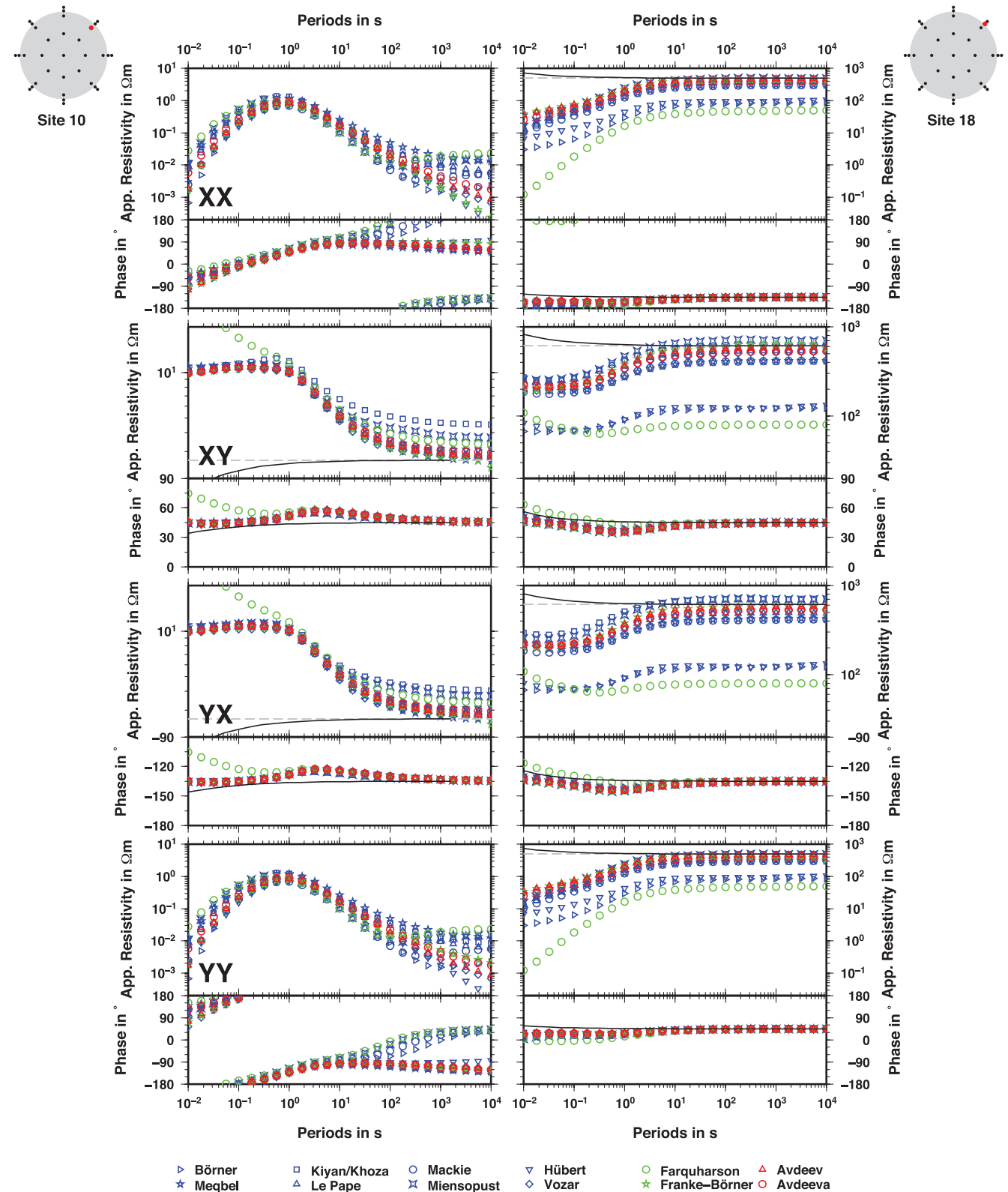


Figure 4. Comparison of the obtained DTM2 responses. From top to bottom each row shows the xx , xy , yx and yy components (i.e. apparent resistivity and phase curves). The left column shows the responses at site 10 whose location is indicated by the red dot in the small sketch on the top left (inside the hemisphere; at surface 500 m away from the edge). Similarly, the red dot in the sketch on the top right indicates the location of site 18 (outside the hemisphere, at surface 100 m away from the edge), whose responses are shown in the right column. The grey dashed line represents CZ and the solid black line the analytic solution calculated by David Bosch (after Groom & Bailey 1991). (Note that both are indeterminate for diagonal elements at sites inside the hemisphere.) Blue symbols represent responses obtained by FD codes, green symbols those by FE codes and the IE responses are in red. More details can be found in Table 4 and in the text.

each code) and a comparison of their advantages and disadvantages is given.

One important part of inverse numerical modelling is to determine the measure of the misfit. The sum of the measures of data misfit and model complexity is called an objective function (or a penalty function). These measures are often defined by an L-norm, but also non-standard norms and measures are used. The objective function is the sum of these measures balanced, or ‘regularized’, by a trade-off parameter and therefore often is called Tikhonov regularized penalty function. It is this function that will be minimized using CG, NLCG, GN or QN methods.

3.2 Dublin Test Model 1 (DTM1)

In Section 2.2 (see also Fig. 1 and Table 1), this model was described in detail. To illustrate the range of data, Fig. 5 shows pseudo-sections of resistivity and phase values of all four components along the centre profile using the data set calculated by Miensopust utilising the code by Mackie *et al.* (1994). The diagonal resistivity and phase values are blanked in these pseudo-sections if the resistivity of the component is less than a threshold value of $10^{-5} \Omega\text{m}$ (see above). Although the model is relatively simple, the pseudo-sections show increasing resistivities for the diagonal elements that are only a few orders of magnitude smaller than the off-diagonal resistivities. Already the pseudo-sections indicate that there is a more conductive structure a few kilometres below the surface and another one deeper and shifted to the right (positive side of the y axis). Mackie inverted the synthetic data using the FD code of Mackie *et al.* (2001). Table 5 lists the different settings and mesh parameters that were used for the inversion, as well as information regarding run time and final misfit. As expected, his inversion result (see Fig. 6) recovers the lateral extent and the top of the shallow conductor (body 1 in Fig. 1) very well. The lower conductor (body 2 in Fig. 1) is recognizable in section $x = -7.5 \text{ km}$; the resistive structure is also indicated in the model but not resolved as well as the conductors. It is a general problem that MT data, as with all inductive EM techniques, are more sensitive to conductive structures than to resistive bodies and therefore, while the top of a conductor is well defined, its base is usually smeared out. It is also nearly impossible to reproduce the extreme resistivity contrasts of the true model using a smooth inversion approach, as undertaken here. Rodi & Mackie (2012) used this model to discuss 3-D MT inversion, and illustrate the effect of the regularization parameter resulting in models that vary from overly smooth to extraneous structures. Another challenge of this inversion was the sparse distribution of sites mainly along the edges of the bodies rather than across the structure.

Fig. 7 shows a comparison of Mackie’s forward (red) and inversion (blue) responses. The overall fit is good and therefore in agreement with the achieved final RMS misfit value of 1. Nevertheless, while RMS = 1 suggests that everything is well fit, looking at the comparison of the response curves for this example site (at $x = y = 0 \text{ km}$) clearly illustrates that some periods and components are fit better than others, and there is serial correlation in the residuals. So, ideally one should not just rely on this single number but more carefully examine the misfit over all data space.

3.3 Dublin Test Model 2 (DTM2)

In Section 2.3 (see also Fig. 3 and Table 3) the model was already described. Note that the inversion results obtained are based on data that the person calculated her-/himself during the forward exercise,

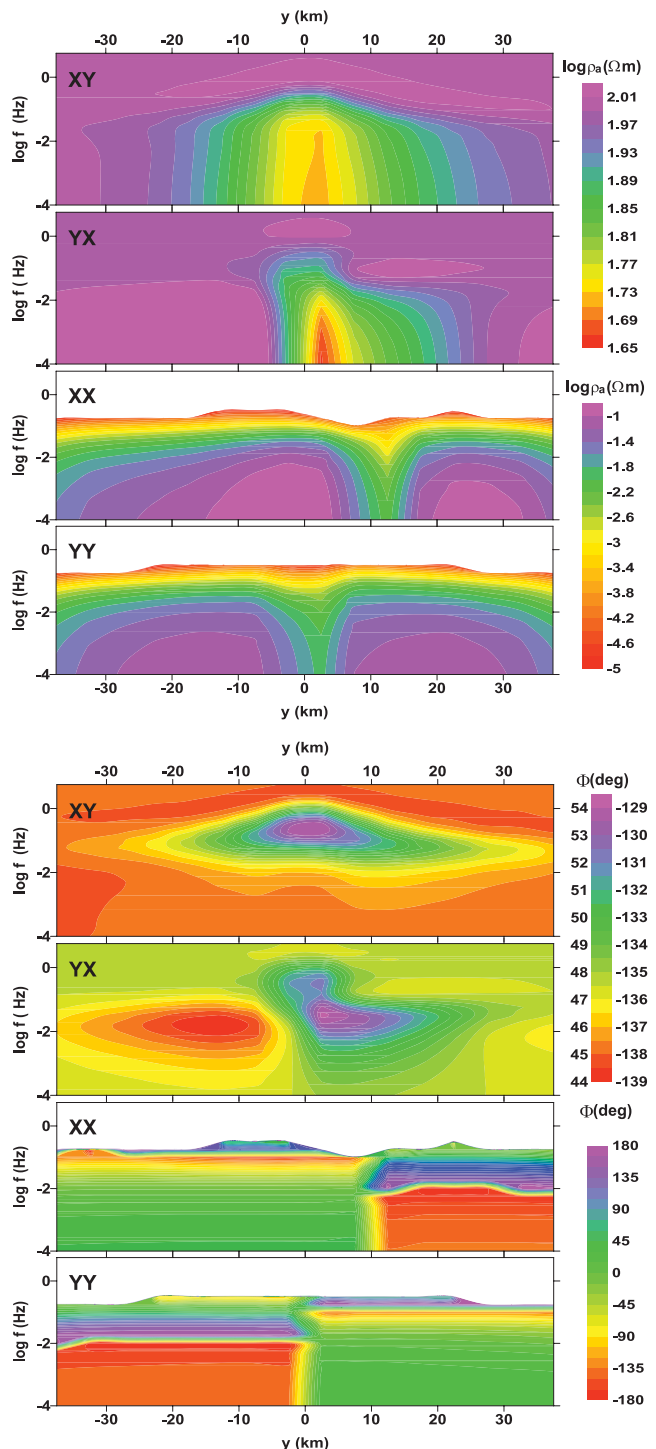


Figure 5. Pseudo-section of DTM1 along the Centre profile (see Fig. 1) using exemplary the data set calculated by Miensopust utilizing the code by Mackie *et al.* (1994). Top panels show the resistivity pseudo-sections for all four components and phase pseudo-sections are below. Note that the diagonal element values are blanked for resistivity and phase if the resistivity values is less than a threshold value of $10^{-5} \Omega\text{m}$.

and therefore the data sets inverted are not identical for the results shown in Fig. 8. While Hübert and Le Pape both started from a homogeneous half-space of $100 \Omega\text{m}$ and used the FD code by Siripunvaraporn *et al.* (2005) and Siripunvaraporn & Egbert (2009), respectively, Avdeeva obtained the model using her IE inversion

Table 5. List of DTM1 inversion results. Beside code and user, information about the used data (sub)set, mesh and inversion parameters are given as well as the number of iterations, final RMS value and target tolerance (TT).

Code/User	Info	Data	Mesh
FD (Mackie <i>et al.</i> 2001) Randall Mackie (parallelization with PETSc: distributes linear system/not exactly domain decomposition)	73 NLCG iterations RMS 1 30 h on cluster TT: $10^{-10} = rtol$ $(r < rtol \cdot b \text{ with } r = b - Ax;$ $b = \text{right hand side; all preconditioned})$	all 59 sites 8 components + tipper 2 periods per decade $\rightarrow 11$ 2 per cent error floors (0.003 on Tz)	$75 \times 96 \times 45$ cells $158 \text{ km} \times 178 \text{ km} \times 128 \text{ km}$ $1 \text{ km} \times 1 \text{ km} \times 100 \text{ m}$ centre cells (vertical extent increasing with depth) starting model: $100 \Omega\text{m}$ half-space

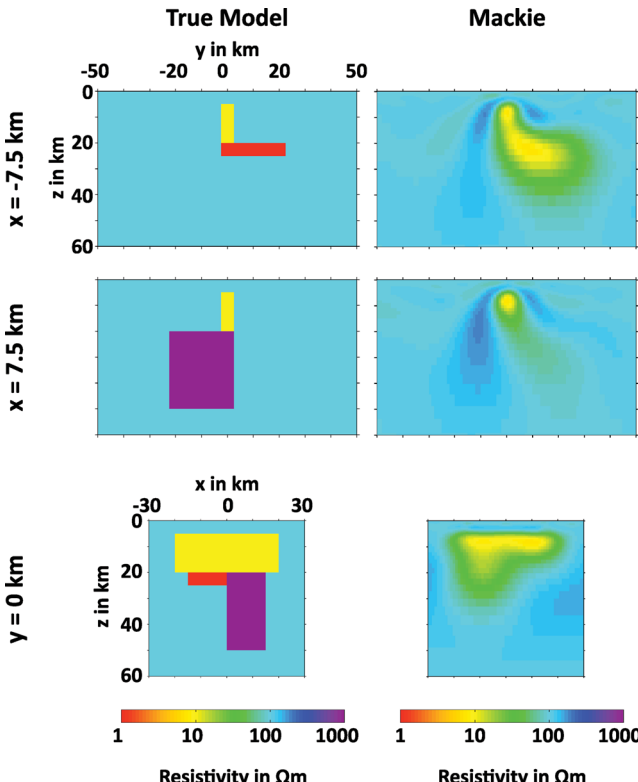


Figure 6. Inversion result obtained for the Dublin Test Model 1 (DTM1). The left column shows slices of the true model. On the right, the same slices are plotted for the inversion model that Randall Mackie obtained using the code by Mackie *et al.* (2001) with the settings specified in Table 5.

code (Avdeev & Avdeeva 2009; Avdeeva *et al.* 2012) starting from the correct half-space resistivity of $300 \Omega\text{m}$. More details about the adopted meshes and data sets, as well as inversion settings, can be found in Table 6. All three inversion results recover the circular shape of the hemisphere well, and all models also indicate the correct order of resistivity for the hemisphere. Similar to the forward results in Section 2.3, rectangular meshing also limits for the inversion the correct representation of the round structure. As all inversion codes used are based on a smooth model approach, the edges of the hemisphere are not represented by a sharp boundary, as in the true model, but by a gradual change in resistivity resulting in a more smeared out structure. Fig. 9 shows a comparison of forward (red) and inversion (blue) response curves for site 10 and 18 (i.e. those discussed in Section 2.2). The columns show a comparison for the inversion data by Avdeeva, Hübner and Le Pape, respectively, each with respect to their own forward data. Although all three obtained an overall RMS misfit of about 1 (see Table 6), Fig. 9 clearly shows how different the fit of those responses curves are. In general, it seems that for all three the data of site 18 (outside the

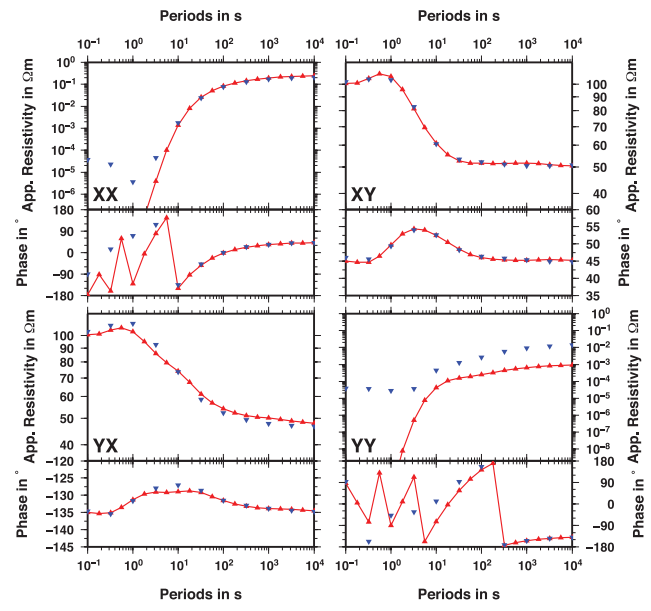


Figure 7. DTM1 comparison of forward versus inversion responses. Presented in red are the forward responses obtained by Randall Mackie at the central site ($x = y = 0 \text{ km}$) and in blue his inversion results. Note that not all periods were used for the inversion and the error floor was set to 2 per cent of the off-diagonal values.

hemisphere) is fit better than for site 10 (inside the hemisphere). While Le Pape's results fit the short periods well and have a bit of a shortcoming on the longer periods, the data obtained by Avdeeva shows the opposite behaviour. Hübner only used short periods, but even for those it is obvious that the fit is different for different components and periods. Once again it becomes clear that a single number RMS misfit is not a satisfying way to represent data fit.

3.4 Dublin Secret Model 1 (DSM1)

3.4.1 Model and data description

Inversion codes are commonly developed and tested by inverting synthetic data from a known structure, but later they will be used to invert real data where the true structure is unknown. To investigate how much the inversion results depend on knowledge of the structure, and therefore, the specifically chosen mesh and parameter settings, we provided a synthetic data set for inversion where the original structure was not known to the participants. (Data set available as supplementary file.) Additional to the data set, the following information was given to them:

- (1) 100 sites on 10 profiles covering a $50 \text{ km} \times 50 \text{ km}$ area (equal site spacing between sites and profiles of 5 km),
- (2) data set covers period range from 0.56 to 10000 s (18 periods),
- (3) expected resistivity range of the structure is 1 – $1000 \Omega\text{m}$,

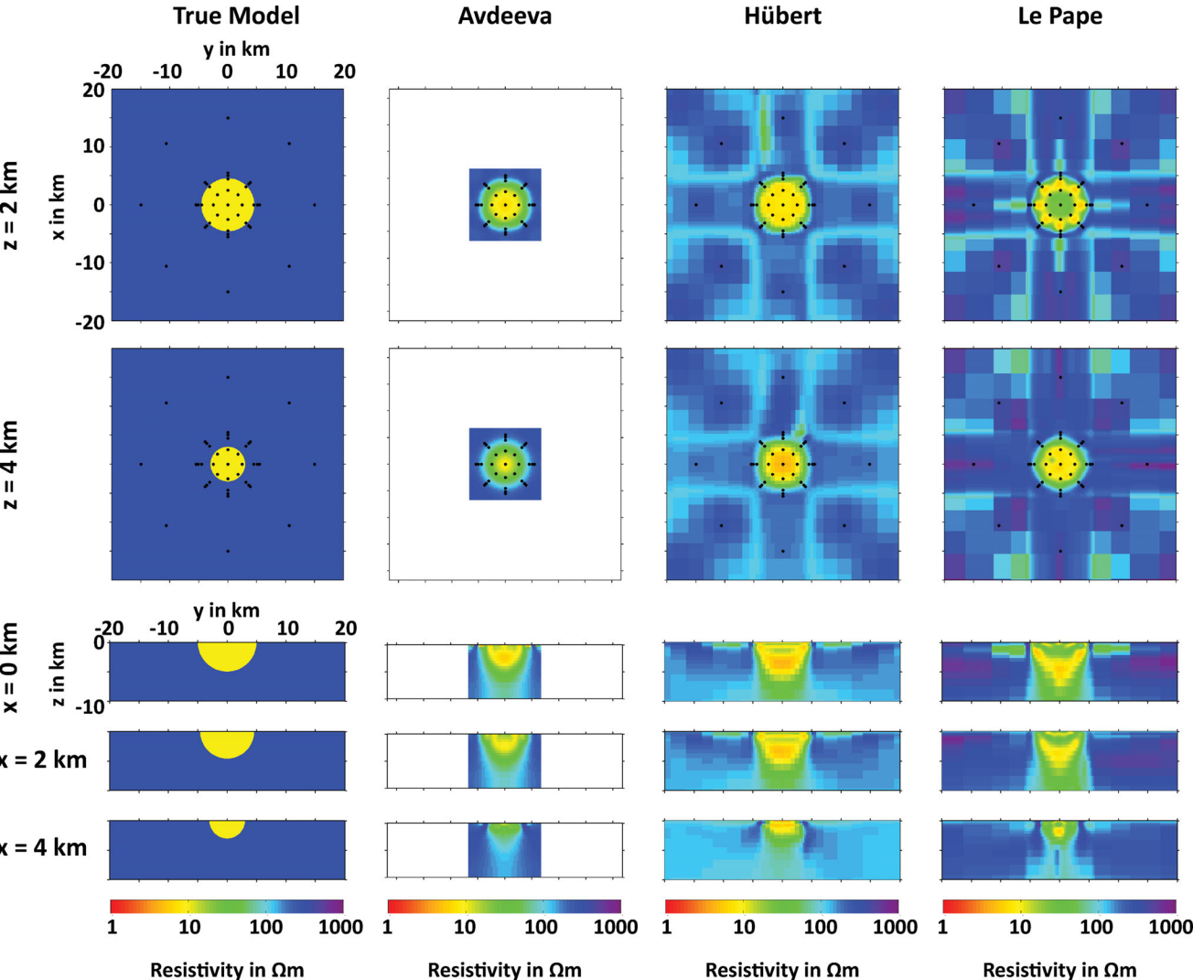


Figure 8. Comparison of the inversion results obtained for the Dublin Test Model 2 (DTM2). From left to right, true model and the inversion results from Anna Avdeeva, Juliane Hübert and Florian Le Pape are shown. The black dots represent the used sites. Table 6 lists the different settings and parameters chosen to obtain the represented models. Note that Anna Avdeeva's model covers a smaller area than the others resulting in the blank area around her model.

(4) impedance values are given in SI units (i.e. Ω) and are based on the $e^{+i\omega t}$ convention,

(5) used coordinate system is x pointing North, y pointing East and z positive downwards,

(6) how many and which sites and periods are used for the inversion was up to individual choice.

The synthetic data were distortion- and noise-free and data errors were not specified. The structure of the model was motivated by finding a synthetic model that results in relatively large diagonal element values, which is not the case for most synthetic data sets. In addition, we were seeking a structure that is different to the block-like structures of most other test models. The chosen structure is a spiral like conductor of $1 \Omega\text{m}$, which becomes thicker and wider with depth (see Fig. 10). Its top is at 4 km depth and both of its ends extend to infinity (i.e. the edge of the forward modelling mesh). Fig. 11 shows resistivity and phase pseudo-sections for all four components at $y = -17.5 \text{ km}$ (across the left part of the spiral). It is obvious that the diagonal resistivities are relatively large—sometimes even of the same order than the off-diagonal elements.

Therefore, the diagonal elements contain information and should not be ignored or rejected during the inversion.

3.4.2 Results

Three 3-D inversion models (Avdeeva using her code (Avdeev & Avdeeva 2009; Avdeeva *et al.* 2012), Hautot using her code (Hautot *et al.* 2007, Hautot *et al.* 2011) and Miensopust using the code by Siripunvaraporn *et al.* (2005)) and one model merged from 1-D models of the determinant at each site (Queralt *et al.*), are shown in Fig. 12. Note that Queralt (and colleagues) and Miensopust did not apply any data analysis, decomposition nor dimensionality check and used default inversion parameters to avoid any manipulation of the inversion result as the true model was designed by (and therefore known to) them. Table 7 lists the different inversion parameters and information about the meshes and data sets used.

The 3-D inversion models recover the near-surface structure well. The deeper part of the structure is more diffuse and laterally shifted. Even the 1-D approach indicates the correct near surface structure, although the conductor is more resistive. Similar to the hemisphere model, the spiral also has a round shape that had to be approximated

Table 6. List of DTM2 inversion results. Beside code and user, information about the used data (sub)set, mesh and inversion parameters are given as well as the number of iterations, final RMS value and target tolerance (TT).

Code/User	Info	Data	Mesh
FD (Siripunvaraporn <i>et al.</i> 2005) Juliane Hübert (serial)	2 iterations RMS 0.9502 14 h	all 49 sites only periods < 56 s error floor 5 per cent of main impedance ($\sigma Z_{xx} = \sigma Z_{xy}, \sigma Z_{yx} = \sigma Z_{yy}$)	$45 \times 45 \times 23$ cells (same as for forward) $80 \text{ km} \times 80 \text{ km} \times 20 \text{ km}$ $\sim 500 \text{ m} \times \sim 500 \text{ m} \times 500 \text{ m}$ centre cells (vertical extent increasing with depth) starting model: $100 \Omega\text{m}$ half-space
FD (Siripunvaraporn & Egbert 2009) Florian Le Pape (frequency parallelization)	3 iterations RMS 1.1594 20 h 24 CPUs on ICHEC cluster Stokes TT: 10^{-7} (forward), 10^{-4} (sensitivities)	all 49 sites 24 periods 8 components error floor 5 per cent	$66 \times 64 \times 42$ cells (same as for forward) $893 \text{ km} \times 893 \text{ km} \times 434 \text{ km}$ $\sim 250 \text{ m} \times \sim 250 \text{ m} \times 200 \text{ m}$ centre cells (vertical extent increasing with depth) starting model: $100 \Omega\text{m}$ half-space
IE (Avdeev & Avdeeva 2009) (Avdeeva <i>et al.</i> 2012) Anna Avdeeva (serial)	RMS 1 77 h Abakus cluster (Intel Xeon X5570@2.93 GHz, 24 GB) filter parameters $a_x = a_y = 3 \rightarrow 8 \rightarrow 3$ regularization: gradient (from 10^{-3} to 10^{-6}) TT: $0.003 \geq \ b - Ax\ /\ b\ $ (system of linear equations: $Ax = b$)	33 sites (0 to 32) 0.1, 0.32, 1, 3.2, 10, 32, 100 s ↓ 0.032, 0.179, 1, 5.59, 32, 179 s error floor 10 per cent of $ Z $	$54 \times 54 \times 16$ cells $13.5 \text{ km} \times 13.5 \text{ km} \times 10 \text{ km}$ $250 \text{ m} \times 250 \text{ m} \times 500 \text{ m}$ cells (vertical extent increasing with depth) starting model: $300 \Omega\text{m}$ half-space

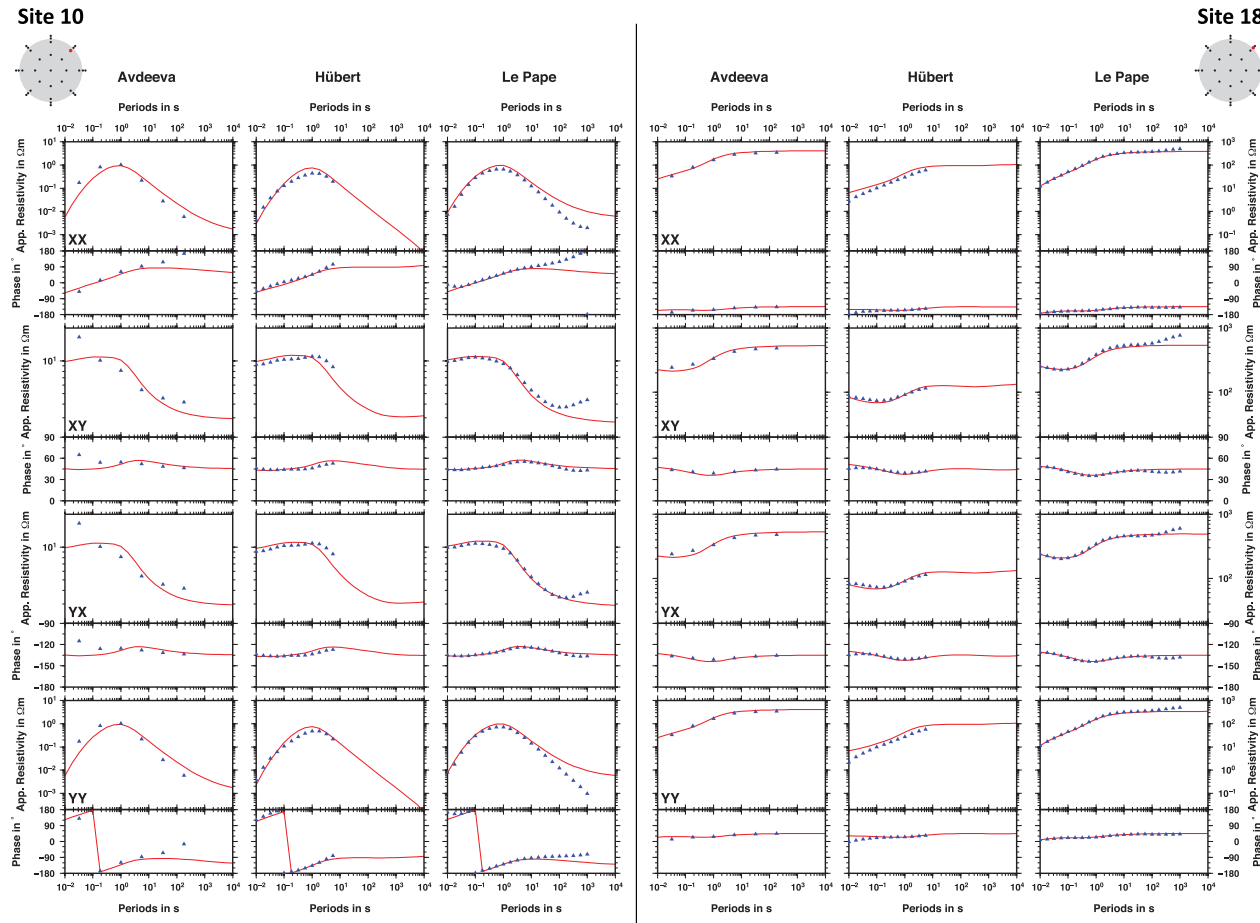


Figure 9. DTM2 comparison of forward versus inversion responses. For the example sites 10 (left) and 18 (right), the data of the inversion (red) obtained by Anna Avdeeva, Juliane Hübert and Florian Le Pape, respectively, are shown in comparison to their forward responses (blue). Although all three obtained an overall RMS misfit of about 1 for their inversion, it is obvious how different the fits are for the different results but also for different periods and components.

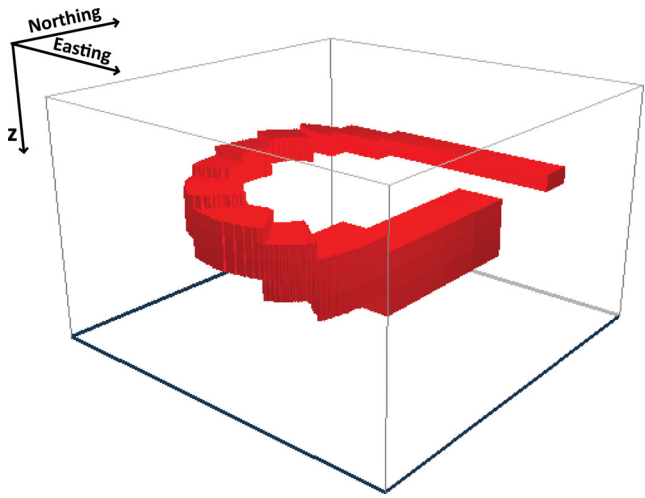


Figure 10. Sketch of Dublin Secret Model 1 (DSM1). The $1 \Omega\text{m}$ spiral (red) is embedded in a homogeneous, $100 \Omega\text{m}$ half-space. Its top is 4 km below surface and its width and thickness increases with depth to a maximum depth of 45.5 km . Both ends extend to infinity, i.e. to the edge of the forward modelling mesh.

by rectangular meshes. It would be interesting to see an inversion using an unstructured grid which probably could reproduce the boundaries a bit better. Nevertheless, the obtained inversion results are promising. Fig. 13 shows pseudo-sections ($y = -17.5 \text{ km}$) of the response data obtained by the three 3-D inversions (i.e. Avdeeva, Hautot and Miensopust). (Note as Queralt *et al.* used a 1-D Occam inversion of the determinant only to see if such a 1-D approach can give a first idea of the structure, no pseudo-sections are shown for their result.) The three pseudo-sections are in a good agreement with the true data (see Fig. 11), although none of the inversions was able to recover the true structure well. All three inversions resulted in similar low RMS misfit values (< 2 , some even around 1), which is an average of the fit of all data points (i.e. all periods and sites). However, inspecting the pseudo-sections clearly shows that differences in the models go back to differences in the fit of each individual data point. As all modellers used all sites, the lateral data distribution is identical for all three models (and also pseudo-sections). While Hautot and Miensopust used (nearly) all periods (17 and 18, respectively), Avdeeva only included half (9) of the periods. For the pseudo-sections, as well as for the inversion models, it seems that the inversion result did not improve with increased number of periods. This might be an effect of the different sensitivities due to diverse inversion algorithms and parameters applied. Note that in this case a reduction in the number of sites would most likely lead to loss of information, and therefore, a worse result. It is obvious that the deeper part of the structure is shielded by the shallower conductive structure. In this case, the resolution of the deeper structure is not improved by using more periods per decade and even a coarse and simple mesh (e.g. the one by Hautot) is able to represent the general structure well. Therefore, a reduced number of periods and/or a simple mesh can be efficient to obtain a sufficient result in a short time and possibly even on a standard laptop.

3.5 Dublin Secret Model 2 (DSM2)

3.5.1 Model and data description

As for the first workshop, we provided again a synthetic data set of unknown structure prior to the second workshop. (Data set available as supplementary file.) The additional information given was:

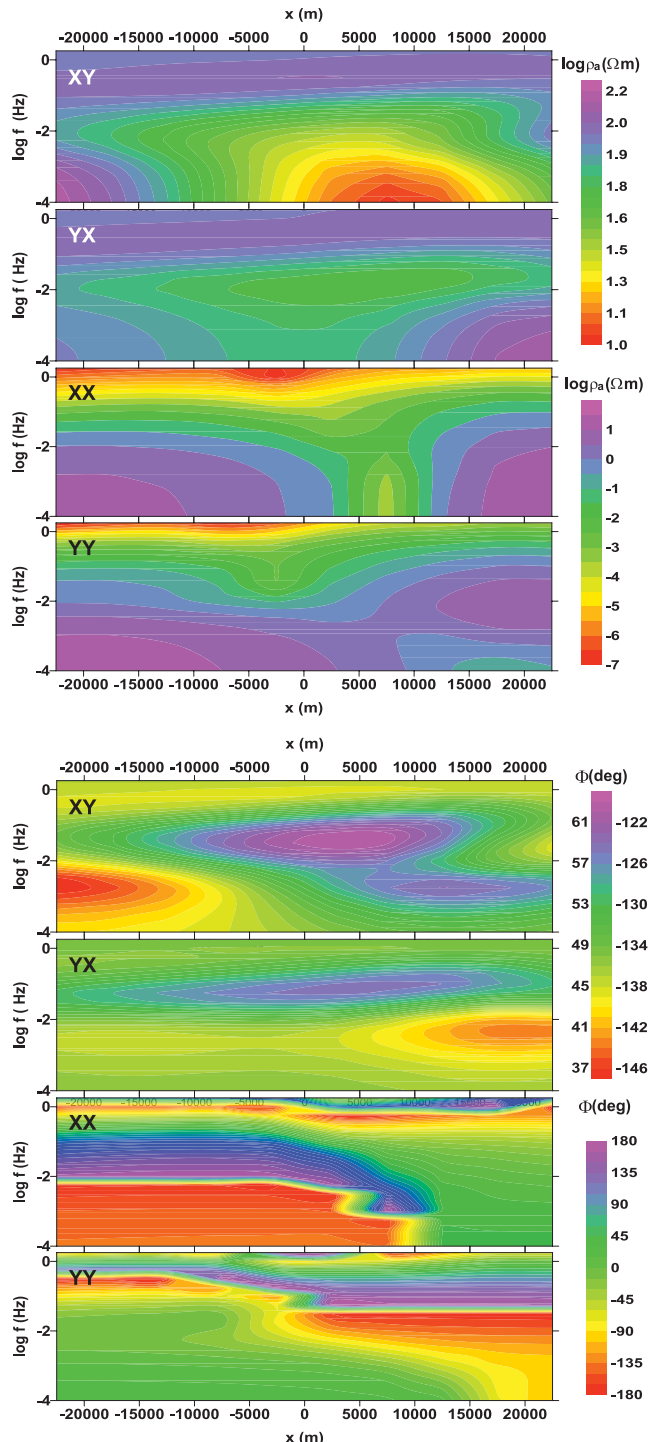


Figure 11. Pseudo-section of DSM1 at $y = -17.5 \text{ km}$. Top panels show the resistivity pseudo-sections for all four components and phase pseudo-sections are below. Note that for some sites and periods, the resistivity values of the diagonal elements are of the same order as those of the off-diagonal elements.

- (1) 144 sites on 12 profiles covering approximately a $80 \text{ km} \times 80 \text{ km}$ area (equal site spacing between sites and profiles of 7 km),
- (2) data set covers period range from 0.016 to $10\,000 \text{ s}$ (30 periods),
- (3) expected resistivity range of the structure is $0.1\text{--}100 \Omega\text{m}$,

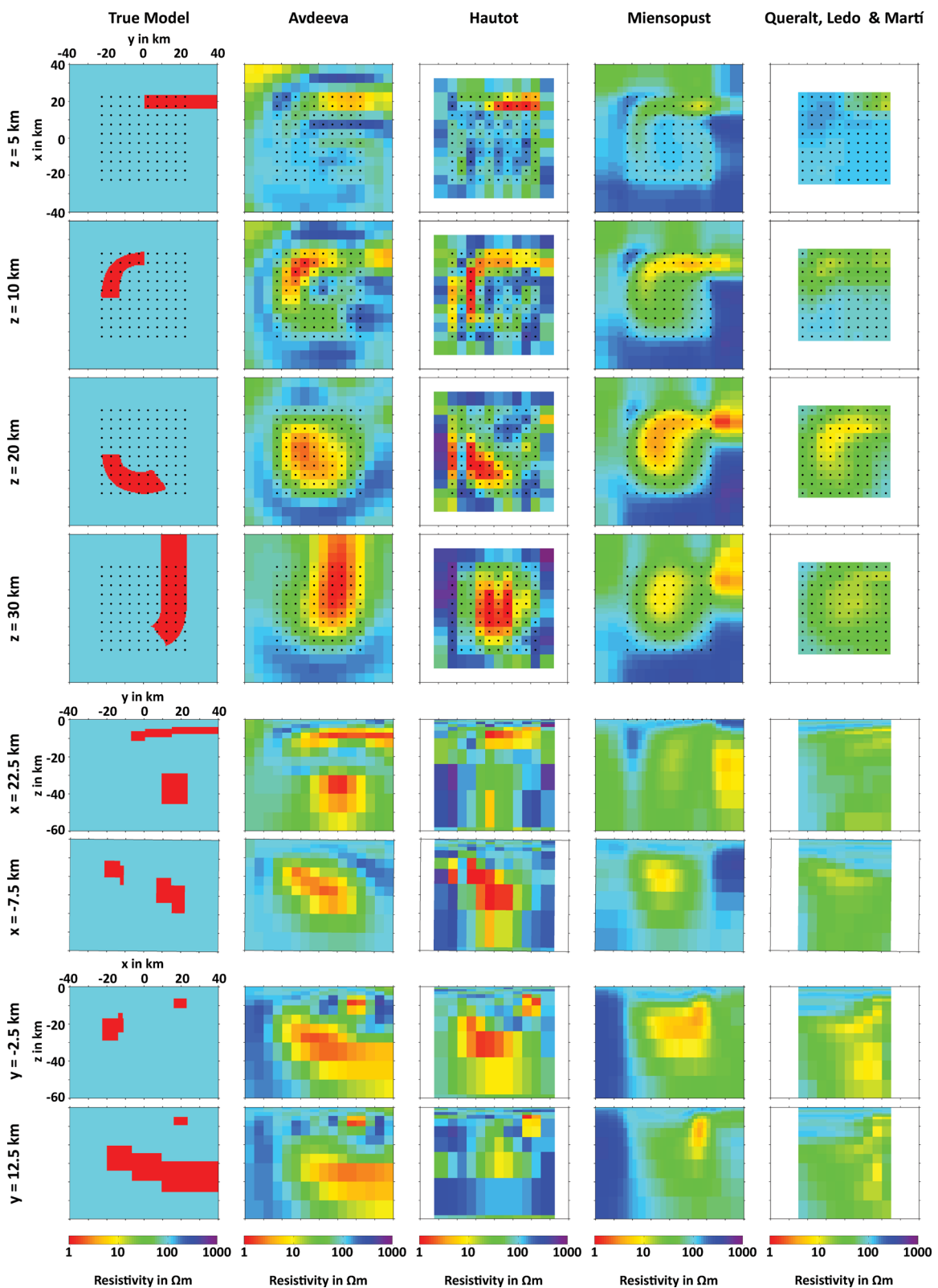
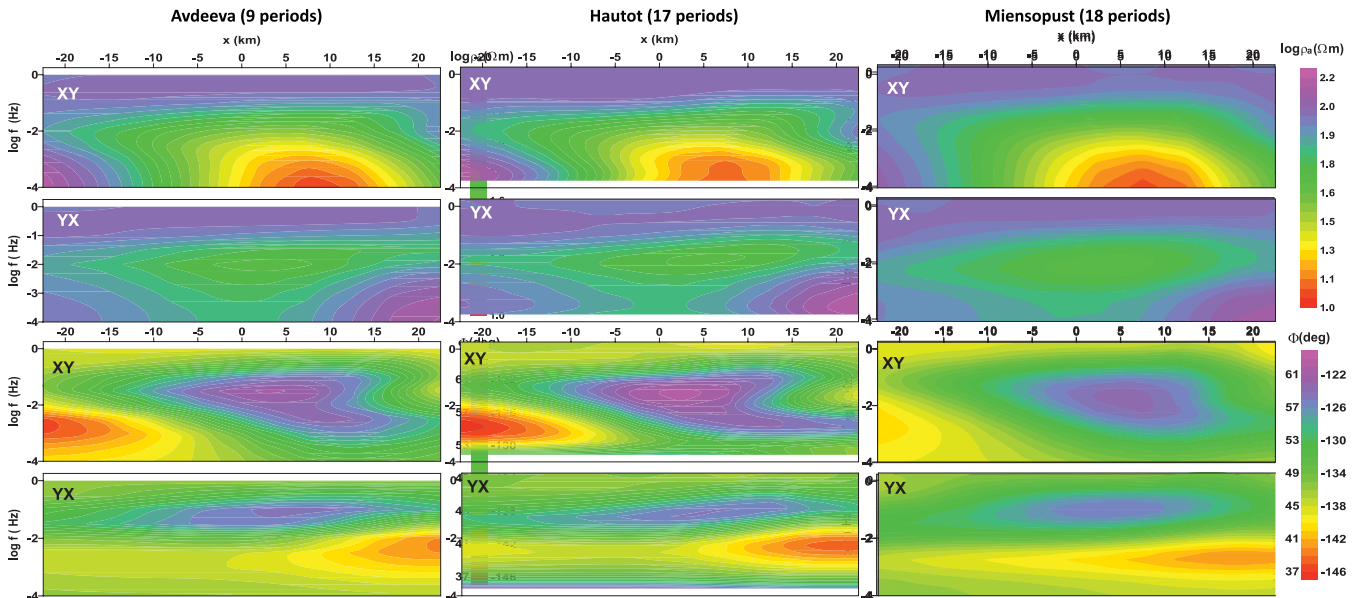


Figure 12. Comparison of the inversion results obtained for the Dublin Secret Model 1 (DSM1). From left to right, the true model and the inversion results from Anna Avdeeva, Sophie Hautot, Marion Miensopust and Pilar Queralt (*et al.*) are shown. The black dots represent the used sites. Note that the model by Queralt *et al.* is not a 3-D inversion model but projection of 1-D models at each site. More details on the used data and mesh as well as information about the inversion parameters can be found in Table 7. White areas indicate where the model extent is less than the plotted area.

Table 7. List of DSM1 inversion results. Beside code and user, information about the used data (sub)set, mesh and inversion parameters are given as well as the number of iterations, final RMS value and target tolerance (TT).

Code/User	Info	Data	Mesh
FD (Hautot <i>et al.</i> 2007, 2011) Sophie Hautot	RMS 1.9 3–4 d standard laptop	8 components all 100 sites 17 periods (without shortest) 2 per cent error floor for off-diagonal 5 per cent error floor for diagonal (or 20 per cent if diagonal $\rho_a < 0.2$) no decomposition	12 × 12 × 12 cells 65 km × 65 × 178 km 5 km × 5 km × 500 m centre cells (vertical extent increasing with depth) starting model: 100 Ωm half-space
FD (Siripunvaraporn <i>et al.</i> 2005) Marion Miensopust (serial)	3 iterations RMS 0.9703 approx. 18 d AMD Opteron CPU 2.193GHz, 16 GB default inversion parameter settings TT: 10^{-7} (forward), 10^{-4} (sensitivities)	8 components all 100 sites all 18 periods no decomposition no dimensionality check no data analysis	44 × 44 × 29 cells 190 km × 190 km × 1130 km 1–2 km × 1–2 km × 100 m centre cells (vertical extent increasing with depth) starting model: 100 Ωm half-space
IE (Avdeeva & Avdeeva 2009) (Avdeeva <i>et al.</i> 2012) Anna Avdeeva (serial)	RMS 1 50 h Abakus cluster (Intel Xeon X5570@2.93 GHz, 24 GB) filter parameters $a_x = a_y = 2$ regularization: gradient (from 10^{-5} to 10^{-7}) TT: $0.003 \geq b - Ax / b $ (system of linear equations: $Ax = b$)	8 components all 100 sites 2 periods per decade → 9 5 per cent error floor	40 × 40 × 15 cells 200 km × 200 km × 100 km 5 km × 5 km × 1 km cells (vertical extent increasing with depth) starting model: 100 Ωm half-space
Occam 1-D (Constable <i>et al.</i> 1987) Pilar Queralt, Juanjo Ledo & Anna Martí	1-D models 19 layers (from 0–60 km) <1 min (standard laptop)	determinant (ρ_a and ϕ) all sites all 18 periods	3-D model constructed from 1D results 10 × 10 cells (5 km × 5 km) each cell represents the 1-D model of one site 1-D starting model: 100 Ωm

**Figure 13.** Pseudo-section of the inversion results of DSM1 at $y = -17.5$ km. Only resistivity and phase pseudo-sections of the off-diagonal elements are shown (compared with true data pseudo-section in Fig. 11) for the results of all three 3-D inversions (from left to right: Avdeeva, Hautot, Miensopust). As the 1-D approach by Queralt *et al.* uses the determinant of the tensor, their resulting data cannot be shown here.

(4) impedance values are given in field units (i.e. $\frac{mV}{km} / nT$) and are based on the $e^{+i\omega t}$ convention,

(5) used coordinate system is x pointing North, y pointing East and z positive downwards,

(6) how many and which sites and periods are used for the inversion was up to individual choice.

The data set was calculated using a model on the basis of the COMMEMI 3D-2A model (Zhdanov *et al.* 1997) but a 1-km thick, near-surface cover layer of 50 Ωm was introduced to avoid numerical problems and effects due to the outcropping structures. While the COMMEMI layered background was kept below the cover layer, the lateral dimensions of the two blocks were modified (see Fig. 14).

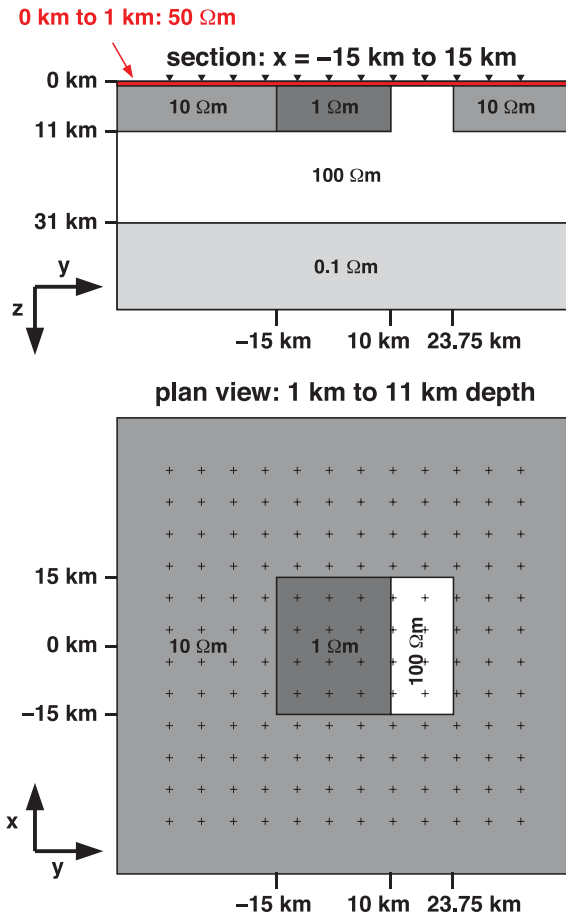


Figure 14. Sketch of Dublin Secret Model 2 (DSM2). A section (top) and a plan view (bottom) show the structures of DSM2. Black crosses in the plan view and triangles in the section view indicate the site locations. This model is on the basis of the COMMEMI 3D-2A model by Zhdanov *et al.* (1997) but with slightly modified lateral dimensions of the two blocks and an additional cover layer.

Then random galvanic distortion was applied to the synthetic data set. Therefore, the distortion matrix C was calculated according to the Groom–Bailey Decomposition (Groom & Bailey 1989) from randomly generated values for the twist angle (within $\pm 60^\circ$), the shear angle (within $\pm 45^\circ$) and the anisotropy (within ± 1). The gain value was fixed to be equal to one at all locations. Finally, random Gaussian noise of 5 per cent of the maximum impedance value was applied to the distorted data set. The given errors were determined as 5 per cent of the maximum values of the absolute impedance values for each period. Fig. 15 shows resistivity and phase pseudo-sections for all four components. The left column represents the synthetic data at $x = 3.5$ km before and the right column after the distortion and Gaussian noise have been applied. Applying distortion and noise enhances the diagonal resistivity values by orders of magnitude (note that the colour scale of undistorted and distorted diagonal resistivities is different).

3.5.2 Results

Table 8 summaries the various inversion codes used, mesh and data selection and inversion parameters of the models shown in Fig. 16. One model was obtained using an IE code (modified version of Avdeev & Avdeeva 2009; Avdeeva *et al.* 2012), all others were

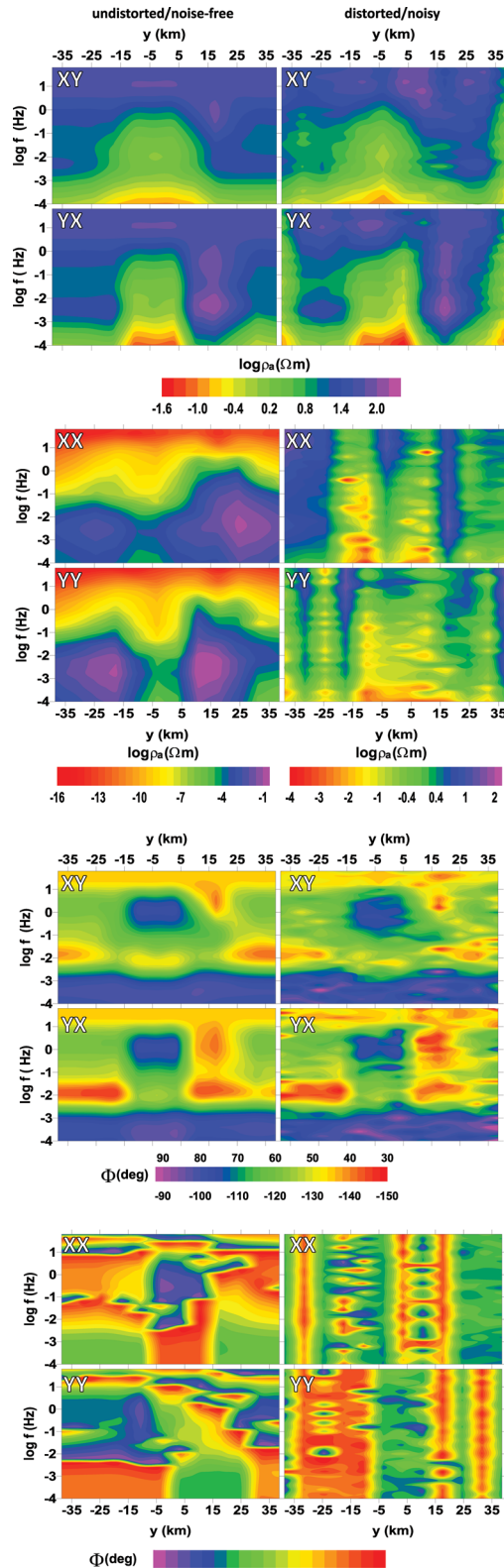


Figure 15. Pseudo-section of DSM2 at $x = 3.5$ km. The left column shows the resistivity and phase pseudo-sections for all four components based on the data as they were obtained by forward modelling. The right column represents the same pseudo-sections after distortion was applied to the data and 5 per cent Gaussian noise was added.

Table 8. List of DSM2 inversion results. Beside code and user, information about the used data (sub)set, mesh and inversion parameters are given as well as the number of iterations, final RMS value and target tolerance (TT).

Code/user	Info	Data	Mesh
FD (Egbert & Kelbert 2012) Naser Meqbel & Gary Egbert	(run A/run B) 262/74 iterations RMS 1.04 /2.5 13/6 h on 31 cores	(run A/run B) 137 sites 15 periods data error = variance/standard deviation	(run A/run B) 50 × 50 × 40/70 × 70 × 48 cells 100/880 km × 100/880 km × 367/914 km 2/3.5 km × 2/3.5 km × 50/5 m centre cells (vertical extent increasing with depth) starting model: 50 Ωm half-space
FD (Hautot <i>et al.</i> 2007, 2011) Sophie Hautot & Pascal Tarits	RMS 4.4 approx. 3 d (desktop PC: 2.5 GHz, 3GB)	all 144 sites all periods no static shift correction 2 per cent error floor for off-diagonal 5 per cent error floor for diagonal (or 20 per cent if diagonal $\rho_a < 0.2$) no decomposition	16 × 16 × 12 cells (2298 unknowns) (cells for layers 10–12 grouped) 133 km × 133 km × 140 km 7 km × 7 km × 60 m centre cells (vertical extent increasing with depth) starting model: 10 Ωm half-space
FD (Mackie <i>et al.</i> 2001) Randall Mackie (parallelization with PETSc: distributes linear system/not exactly domain decomposition)	(No statics/statics) RMS 1.352 / 1.408 NLCG iterations: 62 (10 periods) → 11 (15 periods) → 20 (lower τ, 15 periods)/59 (10 periods) 36/14 h on cluster TT: $10^{-10} = rtol$ ($ r < rtol \cdot b $ with $r = b - Ax$; b = right-hand side; all preconditioned)	142 sites 8 components every 2nd/3rd period → 10/15 (starting at 63.1 Hz) 5 per cent error floor on $\ln Z_{xy}$ & $\ln Z_{yx}$ 20 per cent error floor on Z_{xx} & Z_{yy}	96 × 96 × 67 cells 178 km × 178 km × 107 km 1 km × 1 km × 20 m centre cells (vertical extent increasing with depth) starting model: 10 Ωm half-space
FD (Siripunvaraporn <i>et al.</i> 2005) Xavier Garcia (serial)	2 iterations RMS 4.3104 default inversion parameter settings TT: 10^{-7} (forward), 10^{-4} (sensitivities)	8 components 50 sites 3 periods per decade → 16 (only periods ≤ 1 s or > 10 s) no decomposition no dimensionality check no data analysis	44 × 44 × 33 cells 172 km × 172 km × 102 km 2.33 km × 2.33 km × 50 m centre cells (vertical extent increasing with depth) starting model: 50 Ωm half-space
FD (Siripunvaraporn & Egbert 2009) Marion Miensopust (frequency parallelization)	(run A/run B) 4/6 iterations RMS 3.036 / 4.63 default inversion parameter settings TT: 10^{-7} (forward), 10^{-4} (sensitivities)	(run A/run B) 8 components 64 sites (shifted to cell centre) every second period (≥ 0.063 s) → 14 data error = variance/standard deviation no decomposition no dimensionality check no data analysis	54 × 54 × 30 cells 260 km × 260 km × 326 km 2 km × 2 km × 50 m centre cells (vertical extent increasing with depth) starting model: 100 Ωm half-space
FD (Siripunvaraporn <i>et al.</i> 2005) Oriol Rosell/Pilar Queralt (serial)	13 iterations RMS 3.1 default inversion parameter settings TT: 10^{-7} (forward), 10^{-4} (sensitivities)	4 components all 144 sites 2 periods per decade → 12 no decomposition no dimensionality check no data analysis	20 × 20 × 45 cells 7 km × 7 km × 20 m centre cells (vertical extent increasing with depth) starting model: 100 Ωm half-space
FD (Siripunvaraporn & Egbert 2009) Weerachai Siripunvaraporn (frequency parallelization)	1 iteration RMS 2.9925	4 components all 144 sites 16 periods error floor 10 per cent of $ Z_{xy} Z_{yx} ^{1/2}$ 'triage' and removal of bad data	62 × 62 × 33 cells 230 km × 230 km × 520 km 1.63 km × 1.63 km × 10 m centre cells (vertical extent increasing with depth) starting model: 1 Ωm half-space (various models tested → smallest RMS selected)
FD (Siripunvaraporn & Egbert 2009) Jan Vozar (frequency parallelization)	(run A/run B) 3/4 iterations RMS 3.743 / 3.8164 16/13 h on cluster (24 CPUs on Stokes/ICHEC) default smoothing parameters TT: 10^{-7} (forward), 10^{-4} (sensitivities)	8 components 72 sites (different ones for A & B) 24 periods error floor 5 per cent on impedance	50 × 50 × 50 cells 2795 km × 2795 km × 2275 km 3.5 km × 3.5 km × 50 m centre cells (vertical extent increasing with depth) starting model: 100 Ωm half-space
IE (Avdeev & Avdeeva 2009) (Avdeeva <i>et al.</i> 2012) Anna Avdeeva (modified to invert for full distortion matrix) (serial)	RMS 0.7 152 h (Abakus cluster) filter parameters $a_x = a_y = 3$ regularization: gradient (from 10^{-6} to 10^{-8}) TT: $0.003 \geq b - Ax / b $ (system of linear equations: $Ax = b$)	8 components all 144 sites 3 per decade (≤ 251 s) → 10 ↓ 3 per decade (≤ 3981 s) → 13 error floor 10 per cent of $ Z $	43 × 43 × 14 cells 150 km × 150 km × 70 km 3.5 km × 3.5 km × 250 m cells (vertical extent increasing with depth) starting model: 2 Ωm half-space

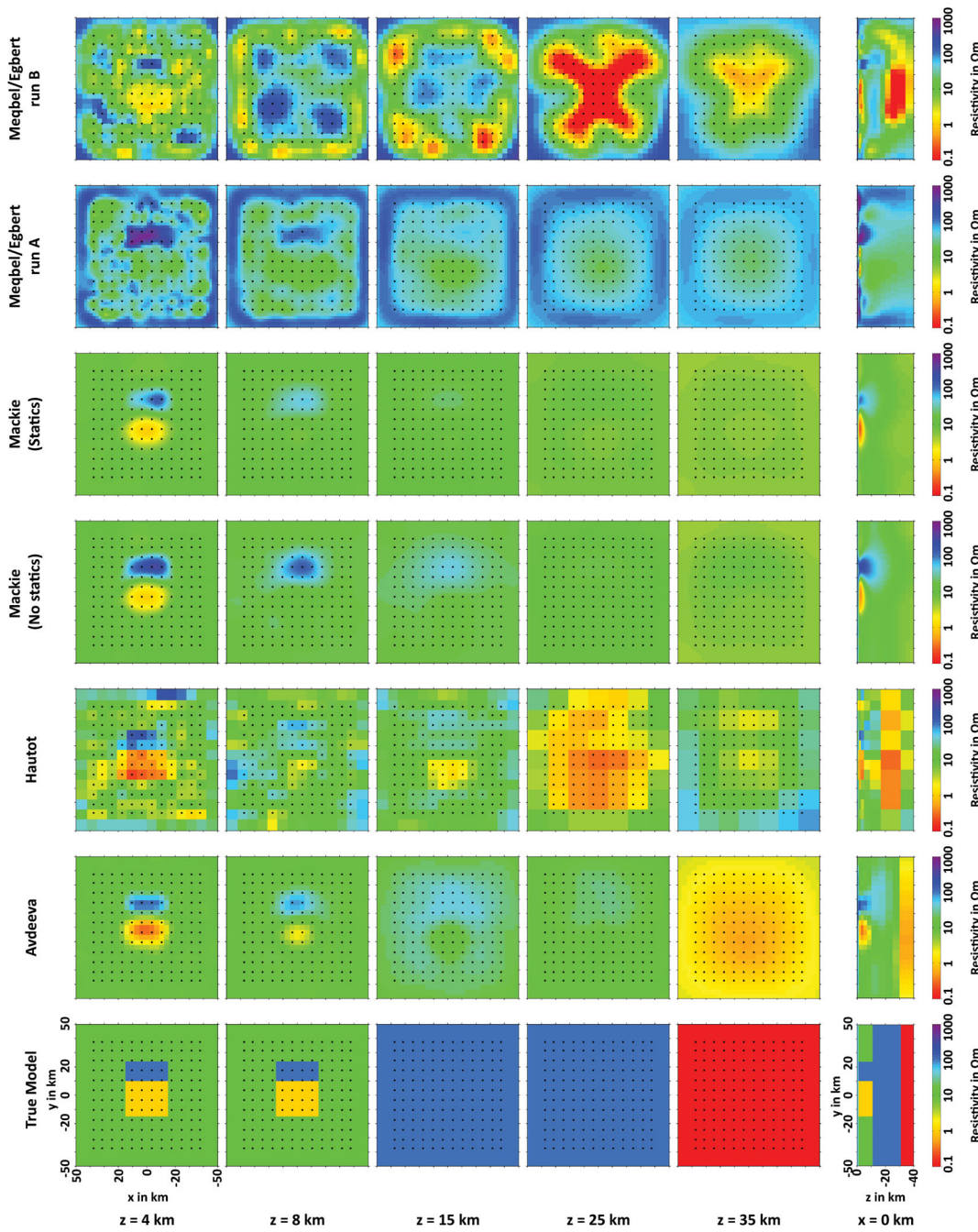


Figure 16. Comparison of the inversion results obtain for the Dublin Secret Model 2 (DSM2). Various inversion results are shown in comparison to the true model. The black dots represent the used sites. More details on the used data and meshes as well as information about the inversion parameters can be found in Table 8. Note that the inversion results by Anna Avdeeva and Randall Mackie (Statics) consider the distortion during the inversion as full distortion matrix and static shift, respectively, while all other results are obtained by inverting for the resistivity structure only. A more detailed discussion of the difference can be found in the text. (Figure continued opposite)

calculated using various FD codes (i.e. Mackie *et al.* 2001; Siripunvaraporn *et al.* 2005; Hautot *et al.* 2007, 2011; Siripunvaraporn & Egbert 2009; Egbert & Kelbert 2012). Although the data set provided also contained information about errors (standard deviation), they were labelled as variance in the file in error, which led to not identical errors used for the various inversions. Some participants used the values as standard deviation (i.e. used the intended errors), others understood the values as variance (i.e. variance = (standard deviation)²), and therefore got unrealistically large errors for long

periods) and others calculated errors themselves or used large error floors for all periods. These differences in errors have, of course, effects on the inversion results, especially whether the deeper structures are resolved or not. The runs A and B by Meqbel and Egbert (slightly different mesh for the two runs) and Miensopust (mesh and inversion settings identical for both runs) show the different models obtained by using the values as variance (run A) or standard deviation/correct errors (run B). This comparison clearly shows that the large errors (when using errors as variance) blank out any

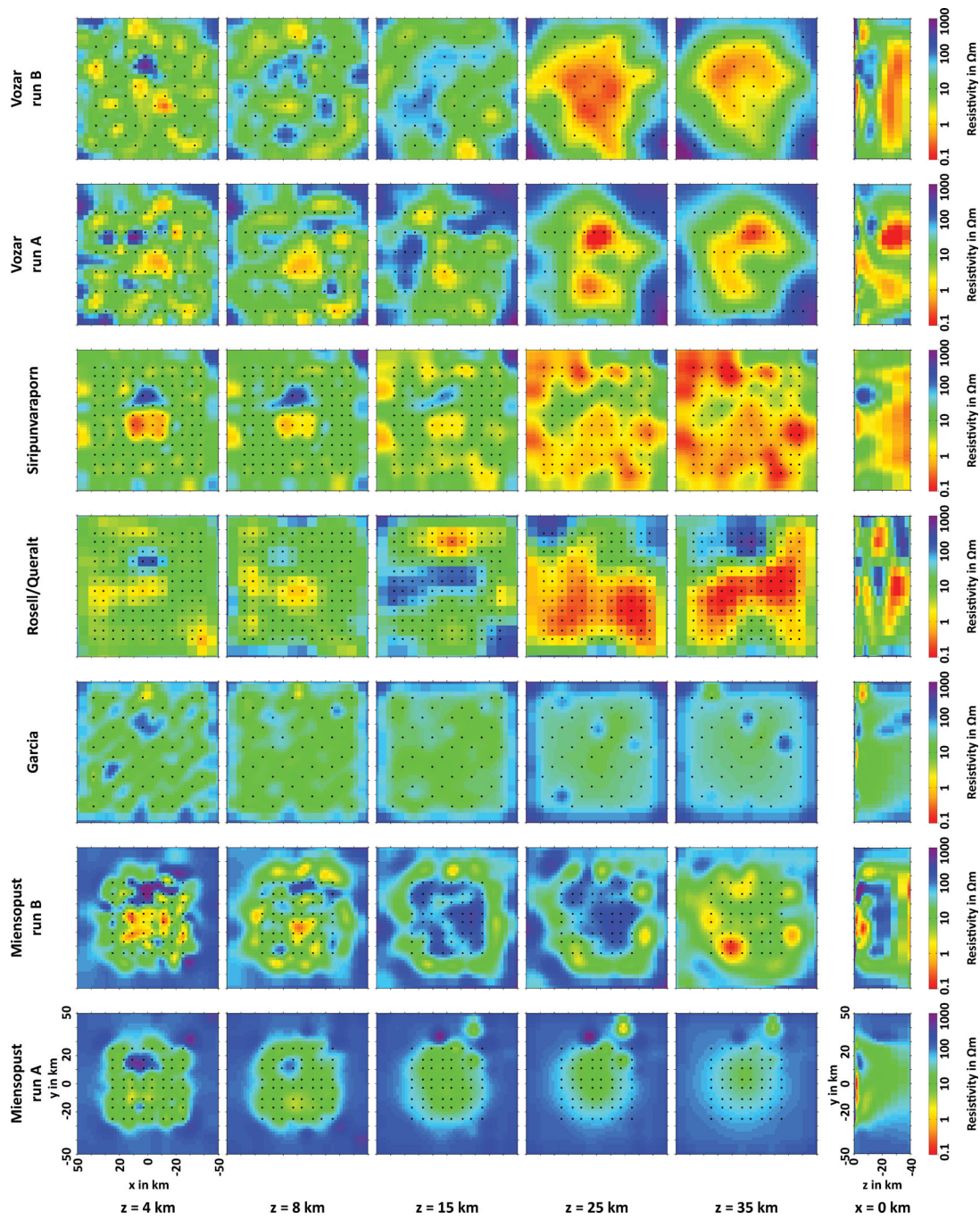


Figure 16. (Continued.)

deep structure in favour of the shallower structure (see sections for the shallow conductors). Therefore, an unresolved lower conductive layer has nothing to do with the inversion algorithm nor the mesh nor inversion parameters, but is caused by the choice of data errors. Although Avdeeva used variance, she obtained the conducting layer at the bottom, but only when overfitting the data (i.e. RMS < 1) as the long periods have large error bars and therefore have a RMS value below 1.

Table 8 also shows that the diagonal elements were treated differently during the inversion. For example, Siripunvaraporn and Rosell/Queralt ignored them and inverted the off-diagonals only; others (e.g. Mackie) used a higher error floor for the diagonals than on the off-diagonals and Hautot defined a threshold value for

the diagonal values below which she assigned a larger error than above. To date, there are only very limited and contradictory ideas about the importance of the diagonal elements for 3-D inversion. Hence, there is also no conclusion yet how to treat them during inversion. The comparison shown here cannot promote one or the other approach, and therefore this topic remains a subject for further investigation.

Another challenge of this data set is the distortion applied. Most inversions ignore distortion effects, or, at most, bad data point elimination was conducted or sites rejected (compare ‘Data’ in Table 8) but no systematic distortion analysis or removal was considered. Avdeeva used a modified version of her code that allows inversion for structure as well as for the full distortion matrix.

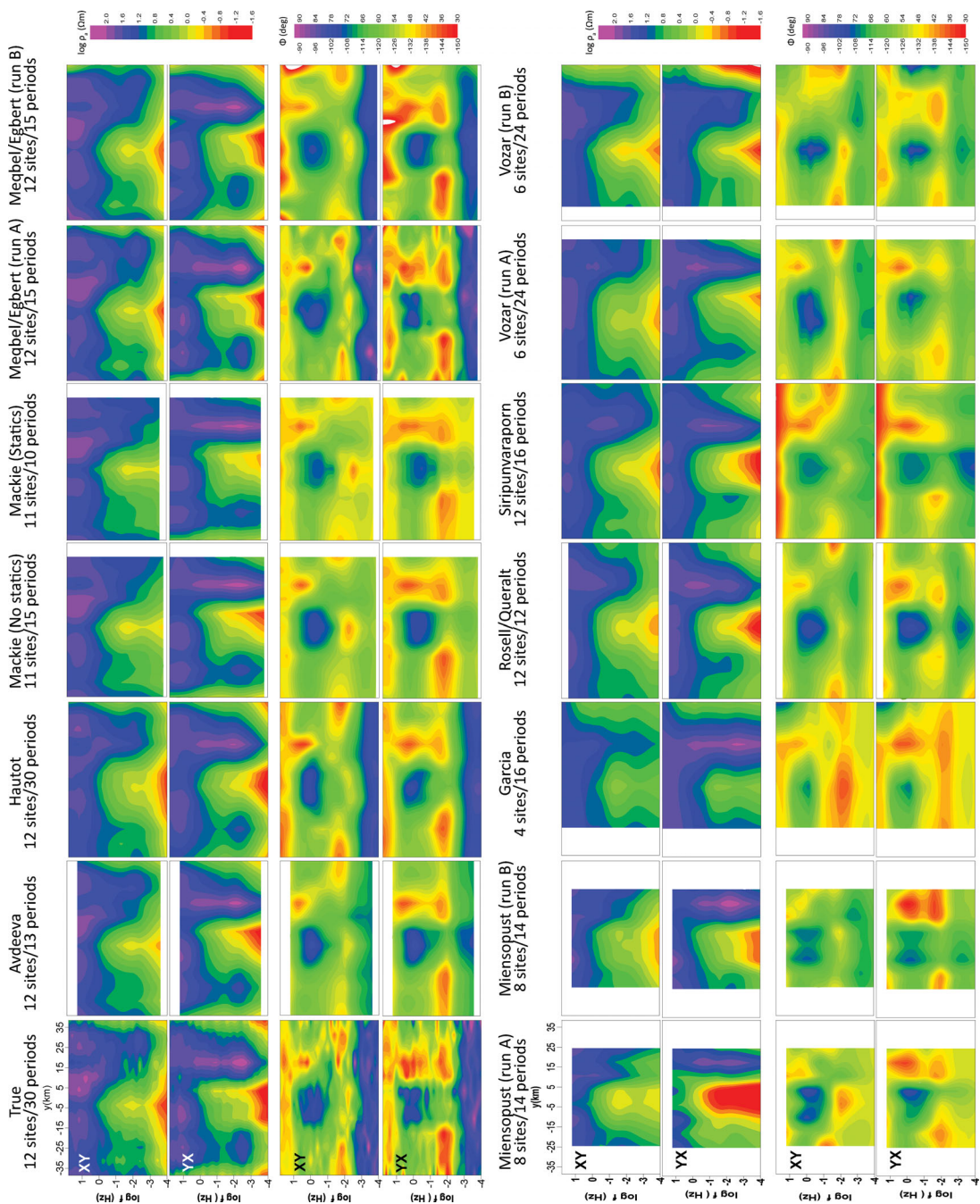


Figure 17. Pseudo-sections of the inversion results of DSM2 at $x = 3.5$ km. For all inversion results shown in Fig. 16, the pseudo-sections of the off-diagonal resistivities and phases (from top to bottom for each set of pseudo-sections: ρ_{xy} , ρ_{yx} , ϕ_{xy} , ϕ_{yx}) are shown in comparison to the true data pseudo-section (i.e. data with distortion and added noise as it was provided). Note that those pseudo-sections are based on different numbers of sites and periods used for the inversion (numbers are specified for each pseudo-section set).

Therefore, the objective function has an additional trade-off term as constraint for the distortion and a modified data misfit term considering the distortion matrix. Mackie provided two inversion results: one with a normal inversion for resistivity structure only (No statics) and one where not the full distortion matrix but the static shift is considered during the inversion process (Statics). (However, the statics correction method applied was incorrect, as discussed by Jones 2011). The two models provided by Vozar only differ by the sites selected for inversion. Although both results show similar general structures, it is obvious that the selected sites influence the obtained model. It seems that for this resistivity structure a chessboard-like

selection of every second site (run B) resolves the layered background better than selecting every second profile (run A). The presence of distortion and overestimating the conductivity of the near surface conductor and underestimating its thickness is the possible cause of a too shallow lower conductive layer/half-space (see e.g. Hautot, Meqbel/Egbert (run B), Rosell/Queralt, Siripunvaraporn, Vozar (run A & B)).

Fig. 17 shows a comparison of the off-diagonal resistivity and phase pseudo-sections for all inversion results shown in Fig. 16 and of the true data (i.e. data with distortion and added noise as it was provided). Note that those pseudo-sections are based on different

numbers of data points for each model (i.e. different numbers of sites and periods). Although the RMS misfit values (see Table 8) are all, more or less, of the same order, once again the pseudo-sections show clearly the difference in fit of the various data points. Most inversion results seem to fit the phases quite well whereas the resistivity values show more discrepancies. Of course, those differences are also subject to the adopted error values and the chosen error floor as well as to the selected data subset (i.e. inversion with or without diagonal elements, rejection of some sites or periods). This once more highlights the need for a better measure of data fit/misfit than just a single number.

Interesting to note is that the models by Mackie ('No statics' and 'Statics') are very similar, but the pseudo-sections are very different. Probably not only the distortion but also structural information in the data has been considered as static shifts by the inversion algorithm, and therefore, the pseudo-sections are overly smooth compared to the 'No statics' inversion and the true data.

In general, the differences in results depend on many things—even if the same inversion code is used, differences can be caused by:

- (1) not only the number but also the distribution of sites (compare, e.g. Garcia versus Rosell/Queralt, Vozar run A versus run B),
- (2) if diagonal elements are ignored (see Rosell/Queralt and Siripunvaraporn) or used (all others),
- (3) selection of errors and error floor; especially in this case, variance versus standard deviation (see run A versus run B of Meqbel/Egbert and Miensopust).

Due to the different usage of the specified error values, it is not possible to judge if more periods improve the results. (Hautot was the only one using all periods whereas everyone else used approximately half of them, but her good result could simply be related to chosen errors/error floor.) A comparison of the results by Garcia and Rosell/Queralt (using the same code) suggest that one cannot gain anything with a finer mesh if only a few data values are used.

Despite all differences, it is obvious that not the numerical algorithms are the weak point but the way they are used, how the data are prepared and selected and how the errors are estimated and used. It seems that all codes returned sufficient results for what they were 'fed' with.

4 DISCUSSION

Although we tried to address a number of issues and were successful at advancing understanding, many still remain unsolved. The exercises emphasized once more that forward and especially inversion algorithms must not be used in a black-box-like manner. Detailed knowledge of the code and the parameters to choose is as essential as triaging the data used. The comparison of the results from DSM2 showed how significant differences in the resulting inversion models can be depending on the used data error and selected error floors. Errors allow emphasis of some model parts and blank out others; therefore they have to be chosen carefully.

It also became clear that a simple RMS misfit is not a satisfying measure of how well the model fits the data. A single number can clearly not represent the data fit and model roughness—not only in 3-D but also in 2-D—in a meaningful way. One approach might be data misfit maps for each impedance tensor element and each period. But no matter how it will be realized, a more sophisticated presen-

tation is required. It would also be beneficial for the community if a common format for model (and data) files could be established and would be used for all available codes. That would allow users to compare results of and move their data and models between different algorithms in a straightforward manner. Currently, numerous conversion scripts have to be used to go back-and-forth between the different formats. But such scripts are always another possible source of errors and mistakes. Perhaps even defining a standard colour map could ease comparison of models from different people and codes, that is, assuming the same maximum and minimum resistivity values for the scale, the same colour would represent the same resistivity value.

As we tried to address specific issues with synthetic models and data sets, it is clear that test data sets should become more realistic, for example, using a more realistic site distribution as in the field hardly ever a perfect 3-D array with equidistant sites is possible or using geological–tectonical driven models. It also seems beneficial to follow the EarthScope example on a more global scale and make measured MT data available for scientific use and code testing. Under www.earthscope.org (last accessed 1 March 2013) one can access the data portal, and also it is intended that data acquired using the instruments of the Geophysical Instrument Pool Potsdam (GIPP) will be available to the public 3 yr after completion of the experiment (www.gfz-potsdam.de/gipp_client last accessed 1 March 2013). We consider this a good start, but more institutes and science foundations should follow these examples.

Applying 3-D inversion codes to real data still raises the question how to process and analyse the data before inversion. For 2-D inversion it is standard practice to analyse distortion parameter and strike direction and apply programs such as *strike* (by McNeice & Jones 2001) to obtain 2-D responses. There are no such procedures established yet for 3-D inversion. Determination of strike direction may not be relevant for 3-D structures but distortion still remains a problem (Jones 2011) and should be taken care of either prior to or during the inversion (e.g. Miensopust 2010). Avdeeva used a similar approach to invert for the resistivity structure and the distortion parameter for the DSM2 data set. Her obtained inversion model is the first showing the successful application of such a joint inversion. It is also known that 2-D isotropic inversion applied to data from an anisotropic Earth can cause significant artefacts in the obtained inversion model (Miensopust & Jones 2011). However, so far it is unknown if adding one dimension will cause the same problem, or if the effects become negligible or are even enhanced.

Using synthetic data the diagonal elements are often very small, but in real data, even though they are a few orders of magnitude smaller than the off-diagonal elements, they are far larger than for the synthetic case. The cause of relatively large diagonal elements in real data is presumably a consequence of imperfect data acquisition, such as instrument noise and inaccuracy, external noise (e.g. wind noise, artificial noise) and distortion. This raises another issue of how diagonal elements should be treated in 3-D inversion. Different ideas were discussed, from not using them at all to always including them all. Probably the most sensible approach is to define a threshold value below which they are rejected (i.e. considered to be below experimental error) and above included in the inversion. But that raises the next question of finding the optimal threshold value and if it is data set dependent. Therefore, the issue of the diagonal elements remains a subject to further investigation.

The models and data sets presented here all focused on the impedance tensor information only and do not include geomagnetic transfer function (also known as tipper) data or interstation magnetic transfer function data. An increasing number of forward

modelling and inversion codes are now including the geomagnetic transfer function data, which can provide valuable additional information about the subsurface structures. Also, other inversion approaches, such as inverting for the phase tensor or invariants (the latter taking all impedance tensor elements into account), are not considered in the presented comparison but might provide a good complement or even an alternative to the presented approaches.

5 CONCLUSION

While Zhdanov *et al.* (1997) concluded in their report that the majority of 3-D forward algorithms belong to the class of IE methods and that the differential equation methods revealed shortcomings in theoretical and practical development, 15 yr later the situation has clearly changed. These days the majority of 3-D codes in use is based on the FD method and an increasing number on the FE method. Only one IE code was presented. Clearly the increased computational power (i.e. speed and memory) has promoted FD codes. Although all three methods have their advantages and disadvantages, we found reasonable qualitative agreement between the results. Also, the number of different forward codes presented in comparison to the few 3-D inversion codes reflect clearly that development in this field is still ongoing. The compilation of the forward and inversion comparison illustrated that a number of issues in modelling and inversion can be dealt with and solved sufficiently, but there are also still various challenges to tackle. It is necessary to continue the comparative calculations for 3-D modelling and inversion. This comprehensive collection of test data sets and test models in combination with all the responses and inversion models obtained by various users and codes is a great opportunity to do so. The COMMEMI models by Zhdanov *et al.* (1997)—still used by many to test their codes—showed how valuable such tools are for the entire community.

ACKNOWLEDGEMENTS

We thank all the other participants for making these two workshops so successful: Masoud Ansari, Sébastien de la Kethulle de Ryhove, Hao Dong, Jimmy Elsenbeck, Mark Hamilton, Jelena Koldan, Markus Löwer, Jan Petter Morten, Laust Pedersen, Estelle Roux, Stewart Sandberg, Jan Schmoldt, Toshihiro Uchida and Wenke Wilhelms. The workshops were kindly financially supported by DIAS (both workshops), EMGS (both workshops), WesternGeco (both workshops) and Zonge (2nd workshop).

MPM was initially supported by a Science Foundation Ireland grant to AGJ (05/RFP/GEO001) and subsequently by DIAS. PQ acknowledges financial support from DIUE (Generalitat de Catalunya) (2007BE-100200) and from MEC (Spanish Government) (PR2007-0436/PR2011-0469) for her several visits at DIAS.

Last, but not least, we thank Weerachai Siripunvaraporn and one anonymous reviewers for their helpful comments on the original version of this manuscript that improved it.

REFERENCES

- Avdeev, D.B., 2005. Three-dimensional electromagnetic modelling and inversion from theory to application, *Surv. Geophys.*, **26**, 767–799.
- Avdeev, D.B. & Avdeeva, A., 2009. 3D magnetotelluric inversion using a limited-memory quasi-Newton optimization, *Geophysics*, **74**(3), F45–F57.
- Avdeev, D.B., Kuvshinov, A.V. & Pankratov, O.V., 2002. Three-dimensional induction logging problems, part I: an integral equation solution and model comparisons, *Geophysics*, **67**(2), 413–426.
- Avdeeva, A.D., Avdeev, D.B. & Jegen, M., 2012. Detecting a salt dome overhang with magnetotellurics: 3D inversion methodology and synthetic model studies, *Geophysics*, **77**, E251–E263.
- Börner, R.-U., 2010. Numerical Modelling in Geo-Electromagnetics: Advances and Challenges, *Surv. Geophys.*, **31**, 225–245.
- Chave, A.D. & Jones, A.G., 2012. *The Magnetotelluric Method: Theory and Practice*, Cambridge University Press, ISBN: 9780521819275.
- Constable, S.C., Parker, R.L. & Constable, C.G., 1987. Occam's inversion—a practical algorithm for generating smooth models from electromagnetic sounding data, *Geophysics*, **52**, 289–300.
- Egbert, G.D. & Kelbert, A., 2012. Computational recipes for electromagnetic inverse problems, *Geophys. J. Int.*, **189**, 251–267.
- Farquharson, C.G. & Miensopust, M.P., 2011. Three-dimensional finite-element modelling of magnetotelluric data with a divergence correction, *J. appl. Geophys.*, **75**, 699–710.
- Farquharson, C.G., Oldenburg, D.W., Haber, E. & Shekhtman, R., 2002. An algorithm for the three-dimensional inversion of magnetotelluric data, in *Proceedings of the 72nd Annual Meeting of the Society of Exploration Geophysicists*, Salt Lake City, Utah.
- Franke, A., Börner, R.-U. & Spitzer, K., 2007. 3D finite element simulation of magnetotelluric fields using unstructured grids, in *Proceedings of the 22nd Colloquium of Electromagnetic Depth Research*, pp. 27–33, eds Ritter, O. & Brasse, H., Decin, Czech Republic, ISSN 0946–7467.
- Garcia, X., Ledo, J. & Queralt, P., 1999. 2D inversion of 3D magnetotelluric data: the Kayabe dataset, *Earth Planets Space*, **51**, 1135–1143.
- Groom, R.W. & Bailey, R.C., 1989. Decomposition of magnetotelluric impedance tensors in the presence of local three-dimensional galvanic distortion, *J. geophys. Res. (Solid Earth)*, **94**(B2), 1913–1925.
- Groom, R.W. & Bailey, R.C., 1991. Analytic investigations of the effects of near-surface three-dimensional galvanic scatterers on MT tensor decompositions, *Geophysics*, **56**(4), 496–518.
- Hautot, S., Singel, R., Waston, J., Harrop, N., Jerram, D.A., Tarits, P., Whaler, K. & Dawes, G., 2007. 3D magnetotelluric inversion and model validation with gravity data for the investigation of flood basalts and associated volcanic rifted margins, *Geophys. J. Int.*, **170**, 1418–1430.
- Hautot, S., Goldak, D., Tarits, P. & Kosteniuk, P., 2011. Three-dimensional magnetotelluric inversion of large data sets: case study of Pasfield Lake Saskatchewan for mineral exploration, GEM Beijing 2011, Beijing, China.
- Jones, A.G., 1988. Static shift of magnetotelluric data and its removal in a sedimentary basin environment, *Geophysics*, **53**, 967–978.
- Jones, A.G., 1993. The COPROD2 dataset: tectonic setting, recorded MT data, and comparison of models, *J. Geomagnet. Geoelectr.*, **45**, 933–955.
- Jones, A.G., 1993. The BC87 dataset: tectonic settings, previous EM results and recorded MT data, *J. Geomagnet. Geoelectr.*, **45**, 1089–1105.
- Jones, A.G., 1993. Introduction to MT-DIW1 special section, *J. Geomagnet. Geoelectr.*, **45**, 931–932.
- Jones, A.G., 2011. Three-dimensional galvanic distortion of three-dimensional regional conductivity structures: comments on “Three-dimensional joint inversion for magnetotelluric resistivity and static shift distributions in complex media” by Y. Sasaki and M. A. Meju (2006), *J. geophys. Res.-Solid Earth*.
- Jones, A.G. & Schultz, A., 1997. Introduction to MT-DIW2 special issue, *J. Geomagnet. Geoelectr.*, **49**, 727–737.
- Ledo, J., 2006. 2-D versus 3-D magnetotelluric data interpretation, *Surv. Geophys.*, **26**, 511–543.
- Mackie, R.L., Rodi, W. & Watts, M.D., 2001. 3-d magnetotelluric inversion for resource exploration, SEG Int'l Exposition and Annual Meeting, San Antonio, Texas.
- Mackie, R.L., Smith, J.T. & Madden, T.R., 1994. Three-dimensional electromagnetic modeling using finite difference equations: the magnetotelluric example, *Radio Sci.*, **29**, 923–935.
- McNeice, G.W. & Jones, A.G., 2001. Multisite, multifrequency tensor decomposition of magnetotelluric data, *Geophysics*, **66**(1), 158–173.
- Miensopust, M.P., 2010. Multidimensional Magnetotellurics: a 2D case study and a 3D approach to simultaneously invert for resistivity structure and distortion parameters, *PhD thesis*, Faculty of Science, Department

- of Earth and Ocean Sciences, National University of Ireland, Galway, Ireland.
- Miensopust, M.P. & Jones, A.G., 2011. Artefacts of isotropic inversion applied to magnetotelluric data from an anisotropic earth, *Geophys. J. Int.*, **187**, 677–689.
- Nam, M.J., Kim, H.J., Song, Y., Lee, T.J., Son, J.-S. & Suh, J.H., 2007. 3D magnetotelluric modelling including surface topography, *Geophys. Prospect.*, **55**, 277–287.
- Newman, G.A. & Alumbaugh, D.L., 2000. Three-dimensional magnetotelluric inversion using non-linear conjugate gradients, *Geophys. J. Int.*, **140**(2), 410–424.
- Oldenburg, D., 1990. Inversion of electromagnetic data: an overview of new techniques, *Surv. Geophys.*, **11**, 231–270.
- Poll, H., Weaver, J.T. & Jones, A.G., 1989. Calculations of voltages for magnetotelluric modelling of a region with near-surface inhomogeneities, *Phys. Earth planet. Inter.*, **53**, 287–297.
- Rodi, W.L. & Mackie, R.L., 2012. The Inverse Problem, in *The Magnetotelluric Method—Theory and Practice*, eds Chave, A., Jones, A.G., Mackie, R.L. & Rodi, W.L., chapter 8, Cambridge University Press, ISBN: 9780521819275.
- Sasaki, Y., 2001. Full 3-D inversion of electromagnetic data on PC, *J. appl. Geophys.*, **46**, 45–54.
- Siripunvaraporn, W., 2012. Three-dimensional magnetotelluric inversion: a introductory guide for developers and users, *Surveys in Geophysics*, **33**(1), 5–27.
- Siripunvaraporn, W. & Egbert, G., 2009. WSINV3DMT: vertical magnetic field transfer function inversion and parallel implementation, *Phys. Earth planet. Inter.*, **173**(3–4), 317–329.
- Siripunvaraporn, W., Egbert, G. & Lenbury, Y., 2002. Numerical accuracy of magnetotelluric modeling: a comparison of finite difference approximations, *Earth Planets Space*, **54**, 721–725.
- Siripunvaraporn, W., Egbert, G., Lenbury, Y. & Uyeshima, M., 2005. Three-dimensional magnetotellurics: data space method, *Phys. Earth planet. Inter.*, **150**(1–3), 3–14.
- Varentsov, I.M., 1998. 2D synthetic data sets (COPROD-2S) to study MT inversion techniques, Presented at the 14th Workshop on Electromagnetic Induction in the Earth. Available from: <http://mtnet.dias.ie/data/coprod2s.html>
- Červ, V. & Pek, J., 1990. Modelling and analysis of electromagnetic fields in 3D inhomogenous media, *Surv. Geophys.*, **11**, 205–229.
- Zhdanov, M.S., Varentsov, I.M., Weaver, J.T., Golubev, N.G. & Krylov, V.A., 1997. Methods for modelling electromagnetic fields: results from COMMEMI—the international project on the comparison of modelling methods for electromagnetic induction, *J. appl. Geophys.*, **37**, 133–271.

SUPPORTING INFORMATION

Additional Supporting Information may be found in the online version of this article:

DSM1.txt Data set of the secret model (DSM1).

DSM2.txt Data set of the secret model (DSM2).

DTM1.txt Response sets of the test model (DTM1).

DTM2.txt Response sets of the test model (DTM2) (<http://gji.oxfordjournals.org/lookup/suppl/doi:10.1093/gji/ggt066/-/DC1>)

Please note: Oxford University Press are not responsible for the content or functionality of any supporting materials supplied by the authors. Any queries (other than missing material) should be directed to the corresponding author for the article.